universität wien

DIPLOMARBEIT

Titel der Diplomarbeit

The Interaction of Convective Storms with Complex Terrain - A Case Study of an Alpine Super-Multicell including a Partly Idealized Modeling Approach

Verfasser

Phillip Scheffknecht

angestrebter akademischer Grad

Magister der Naturwissenschaften (Mag.rer.nat)

Wien, 2013

Studienkennzahl:	A 415
Studienrichtung:	Diplomstudium Meteorologie
Betreuerin:	Univ.-Prof. Dr. Vanda Grubišić

Contents

Chapter 1

Introduction

1.1 Motivation

People are fascinated by convective storms. A large number of people, with no meteorological background, is interested in chasing, documenting, photographing and videotaping thunderstorms. Even those who are not directly interested in the subject often rely on forecasts and severe weather warnings for many different reasons. While convective storms have been a subject of a multitude of research studies, little is known about their interaction with mountainous terrain. However, it is especially in mountainous terrain that these storms can cause the most devastation by triggering flash floods and land slides.
The advent of computers has let to the development of numerical models and the application of numerical simulations to study convective storms. In crecent years, the use of simulations has become increasingly common as the availability of computational resources has grown exponentially. Simple two-dimensional (2-D) simulations used to require require a supercomputer only three decades ago, while nowadays even an average personal computer can handle the fully compressible non-hydrostatic three-dimensional (3-D) simulation of a convective system. The publications on severe convective weather reflect this trend by relying more and more on numerical simulations, increased resolutions, larger domains and more sophisticated methods for handling subgrid scale processes and physics. In regard to these developments it is particularly important to maintain a certain simplicity in simulations in order to identify chains of cause and effect. Such simulations have helped tremendously in understanding the dynamics of convective storms. The goal of this work is to explore the interaction of a mesoscale convective system with complex terrain by conducting a case study of a particular storm event and simplifying the terrain under the convective storm to find out how the terrain influences the convective system.

1.2 Scale and Mechanisms of Deep Moist Convection

According to Markowski and Richardson (2010) on the synoptic scale the coriolis and pressure gradient force are approximately in balance. This scale is characterized by processes whose horizontal extension is much larger than their vertical extension. Planetary Rossby Waves or high and low pressure systems are examples for synoptic scale phenomena. In the microscale the coriolis force and sometimes even the horizontal pressure gradient force can usually be neglected. Between these two lies the mesoscale. Markowski and Richardson (2010) describe the mesoscale as "an intermediate range of scales in which few, if any, simplifications to the governing equations can be made, at least not simplifications that can be applied to *all* mesoscale phenomenona." The horizontal exntent of mesoscale phenomena ranges from $\mathcal{O}(1\text{ km})$ to $\mathcal{O}(1000\text{ km})$. Deep convection, which refers to convection that reaches into the upper troposphere, is a mesoscale phenomenon.

1.2.1 Temperature, Pressure and Density

Since the air is in good approximation an ideal gas, temperature, density and pressure are linked by the ideal gas law

$$p = \rho R T, \tag{1.1}$$

where p and T are pressure and temperature, R is the specific gas constant, which is approximately 287 J kg^{-1} K^{-1} for dry air (Holton, 2004) and ρ is the density of the gas. In the ideal case of an atmosphere with no vertical acceleration the vertical component of the pressure gradient compensates the gravitational force. Such a state is described by the hydrostatic equation

$$\frac{dp}{dz} = -\rho g, \tag{1.2}$$

where g is the gravitational acceleration and z is the height.

1.2.2 Instability

Natural convection is driven by buoyancy which is a force caused by density differences. Buoyancy b is given by

$$b = \frac{T_{parcel} - T_{env}}{T_{env}}. \tag{1.3}$$

The potential temperature θ of an air parcel is its temperature after adiabatic compression from p, T to p_s, θ. For an ideal gas θ is given by

$$\theta = T \left(\frac{p_s}{p} \right)^{\frac{R}{c_p}}, \tag{1.4}$$

where c_p is the heat capacity of air for constant pressure. Following Holton (2004), a relationship between the $d\theta/dz$ and dT/dz can be obtained. The logarithm of the definition of potential temperature (1.4) is taken and differentiated with respect to height. Using

the ideal gas law (1.1) and the hydrostatic equation (1.2) the result is

$$\frac{T}{\theta}\frac{d\theta}{dz} = \frac{dT}{dz} + \frac{g}{c_p}. \tag{1.5}$$

The symbol Γ is used for the environmental lapse rate of temperature $-dT/dz$. If θ is constant with respect to z, the lapse rate is

$$-\frac{dT}{dz} = \frac{g}{c_p} \equiv \Gamma_d, \tag{1.6}$$

which is called dry adiabatic lapse rate. Usually the value of Γ is lower than that of Γ_d. Any dry air parcel which is vertically and adiabatically displaced in an atmosphere where $dT/dz = \Gamma_d$ will experience no buoyant forces since it will have the same temperature as its environment at any vertical level. For this case $d\theta/dz$ is 0. If $d\theta/dz > 0$ a parcel will become negatively buoyant when displaced upward and positively buoyant when displaced downward and forced back to its equilibrium level. For the case where $d\theta/dz < 0$, any parcel displaced upward (downward) will become positively (negatively) buoyant. In this case buoyancy will force the parcel to accelerate away from its equilibrium level. This case is called statically unstable. The vertical change of θ with height determines statical stability for dry air.

$$\frac{d\theta}{dz}\begin{cases} > 0 & \text{statically stable} \\ = 0 & \text{statically neutral} \\ < 0 & \text{statically unstable} \end{cases} \tag{1.7}$$

Static instability immediately causes convective overturning and is practically not present on the synoptic scale. Instead it is relevant in smaller scale processes like dry boundary layer convection over warm soil, which can also play a role in the initiation of convective storms. However, the layer characterized by $d\theta/dz < 0$ is usually very shallow compared to the troposphere.

The behaviour of undersaturated and dry air is very similar during a lifting process. However, a rising moist air parcel eventually reaches saturation at its lifting condensation level (LCL). If the rising continues, condensation occurs. Latent heat is then converted into sensible heat which slows the cooling process. The equivalent potential temperature θ_e is the potential temperature that a parcel would have if all its water vapor was condensed and the released latent heat was used to warm the parcel, which is then compressed to p_s. It is approximately given by

$$\theta_e \approx \theta e^{\frac{L_c q}{c_p T}}, \tag{1.8}$$

where L_c is the latent heat of condensation, q is called the specific humidity, which is given by the ratio of mass of water vapor to the mass of moist air, c_p is the heat capacity for constant pressure and T is the temperature. (Hantel, 2006). The temperature change during the ascent of a saturated parcel is described by the pseudoadiabatic lapse rate

(Holton, 2004). It is assumed that supersaturation does not occur and the excess water vapor condenses immediately with the latent heat being converted into sensible heat of the air parcel.

$$\Gamma_s = -\frac{dT}{dz} = \Gamma_d \frac{\left[1 + L_c q_s/(RT)\right]}{\left[1 + \epsilon L_c^2 q_s/(c_p R T^2)\right]}. \tag{1.9}$$

In an environment characterized by $-dT/dz = \Gamma_s$ any saturated parcel which is displaced upward will experience no buoyant force and have the same temperature as its environment at any level. However, if the condensed water is assumed to fall out of the parcel immediately, any downward displacement would desaturate the parcel and cause it to warm with the dry adiabatic lapse rate. The lifting process is irreversible due to the loss of condensed water. The sinking parcel would become positively buoyant and rise back to its equilibrium level.

An atmosphere with a lapse rate of $\Gamma_s < \Gamma < \Gamma_d$ is statically stable but unstable to upward displacement of saturated air parcels. It is reasonable to define the saturation equivalent potential temperature θ_e^* which is the equivalent potential temperature of a saturated atmosphere and is given by

$$\theta_e^* \approx \theta e^{\frac{L_c q_s}{c_p T}}, \tag{1.10}$$

where q_s is the saturation specific humidity. Note that for any unsaturated air parcel $T < \theta < \theta_e < \theta_e^*$ holds, if it is not displaced to a level where $p > p_s$. The pseudoadiabatic lapse rate can also be characterized by $d\theta_e^*/dz = 0$.

$$\frac{d\theta_e^*}{dz} \begin{cases} > 0 & \text{conditionally stable} \\ = 0 & \text{conditionally neutral} \\ < 0 & \text{conditionally unstable} \end{cases} \tag{1.11}$$

The necessary condition for this type of instability is saturation. Since a conditionally unstable atmosphere can be statically stable, conditional instability can form and exist over a long time before it is removed by convection or warm air advection in the mid and upper levels. Conditional instability can also cover large areas extending up to several thousand square kilometers and more. Such large areas are necessary for the formation of large organized convective systems.

1.2.3 CAPE and CIN

Since a rising parcel cools according to the dry adiabatic lapse rate, it becomes negatively buoyant because usually $\Gamma < \Gamma_d$. Only if it is forced to rise to its lifting condensation level (LCL), saturation occurs and the cooling slows. The amount of energy required to push an air parcel with a mass of one kilogram through the layer of air where it is negatively buoyant is called convective inhibition (CIN). It can be obtained by integrating buoyancy

b from the bottom level z_0 to the level of free convection (LFC) where b becomes zero.

$$CIN = g \int_{z_0}^{z_{LFC}} b \, dz. \tag{1.12}$$

In rising saturated air latent heat is released and warms the parcel. If conditional instability is present, the parcel cools at a lower rate than the environmental air. At the LFC the parcel becomes positively buoyant. If the layer characterized by $\Gamma_s < \Gamma < \Gamma_d$ is deep enough the parcel can now rise up into the upper troposphere, gaining more kinetic energy as it rises. Neglecting entrainment and friction, the parcel reaches its maximum vertical velocity at its equilibrium level (EL), close to the tropopause. The total amount of kinetic energy available from buoyancy is called convective available potential energy (CAPE) and is given by

$$CAPE = g \int_{z_{LFC}}^{z_{EL}} b \, dz. \tag{1.13}$$

The above definitions will yield positive values for CAPE and negative values for CIN. However, in many cases both values are given with positive signs. In the sections below the CIN will also be referred to as being positive. If entrainment and friction are neglected, CAPE and CIN correspond to the kinetic energy gained or lost by a parcel while moving upward. Following this analogy, we can calculate the maximal vertical velocity of a parcel after moving through a conditionally unstable atmosphere up to the EL. For simplicity, let us assume the mass of the parcel to be 1 kg, thus

$$E_{kin} = \frac{w^2}{2} = CAPE. \tag{1.14}$$

If friction and entrainment are neglected, the parcel will reach its highest velocity at the equilibrium level, where

$$w = \sqrt{2 \cdot CAPE}. \tag{1.15}$$

For CAPE = 1000 J kg^{-1} this value is approximately 44 m s^{-1}. In the Great Plains values of CAPE over 5000 J kg^{-1} have been estimated which would theoretically allow vertical velocities of 100 m s^{-1}. In reality the values of w are generally smaller.

1.2.4 Vertical Wind Shear

In a conditionally unstable environment which has a vertically homogeneous wind profile convective storms usually develop into short-lived single convective cells. After about 30 minutes water loading, which refers to an increasing mass of rain water per volume, and evaporative cooling cause a downdraft in the center of the cell which cuts off the supply of warm moist air. Only under extremely unstable conditions, involving a very small CIN can the cold outflow trigger secondary cells. Such storms are usually not very strong and unable to produce dangerous levels of precipitation or severe winds.

Larger and more complex convective storms require dynamics which is only supported by certain vertical wind profiles. What is required is the change of the environmental wind $\mathbf{v} = \mathbf{v}(z)$ with height. Vertical wind shear can be described in various ways. The simplest way is to consider the difference between the wind vectors at two different levels z_1 and z_2, where $z_1 < z_2$ and $\mathbf{v}_s = \mathbf{v}(z_2) - \mathbf{v}(z_1)$. In this case $\mathbf{v}_s$ is a vector. The most commonly used is the 0-6 km vertical wind shear which is given by the scalar value $|\mathbf{v}_s|$. A linear change in wind from 0 m s^{-1} at the ground level to 30 m s^{-1} at 6 km in a straight hodograph equals to the 0-6 km shear of 30 m s^{-1}. If expressed as the change of $\mathbf{v}$ with height $d\mathbf{v}(z)/dz$, the unit of wind shear is m s^{-1} m^{-1} = s^{-1}. In the example above, the vertical wind shear equals 0.005 s^{-1}.

Vertical wind shear influences storms in complex ways. Consequently, looking only at the

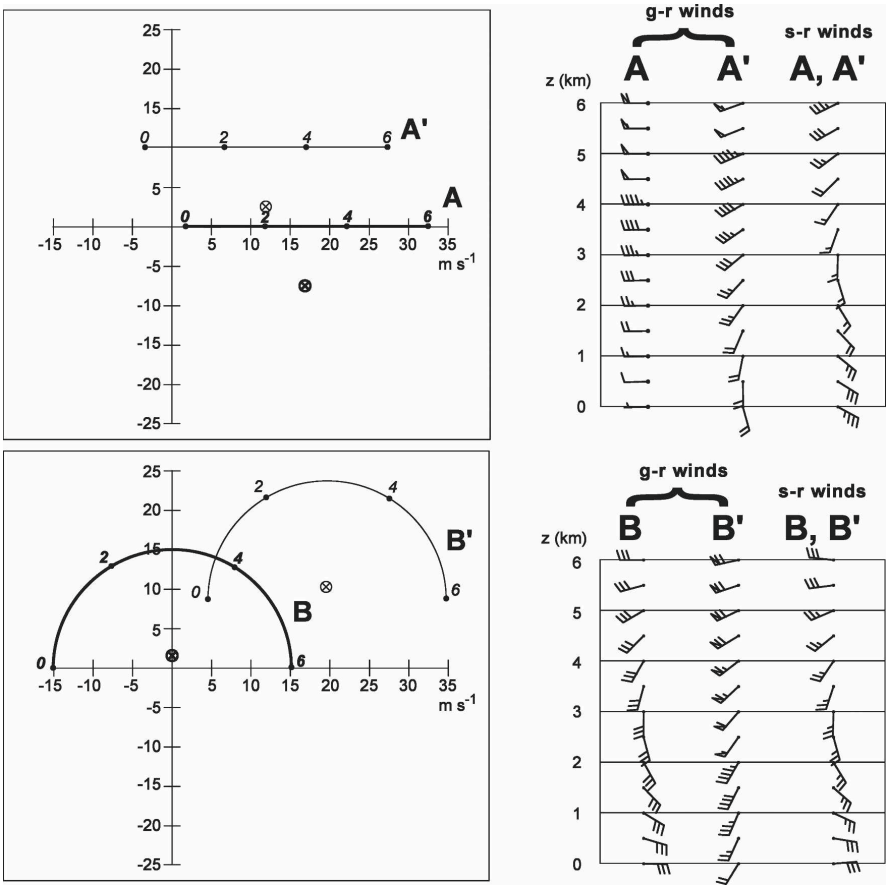

Figure 1.1: Idealized straight (top left) and curved (bottom left) hodographs. The axes show u and v components of the wind in $m\ s^{-1}$. To the right the corresponding ground relative (g-r) and storm relative (s-r) winds are shown by wind barbs. They point in the direction, where the wind is coming from and short (long, bold) dashes indicate the wind speed in 5 (10, 50) knots, the total wind speed is obtained by adding all the values. The symbol $\otimes$ indicates the storm motion vector. Figure from Markowski and Richardson (2006).

difference in wind speed at two seperate levels is not sufficient to understand its impact. The wind profile can vary not only in speed but also in direction with height, which is

why the terms speed shear and directional shear were adopted in literature. However, according to Markowski and Richardson (2006) the use of these terms is often ambiguous. The term directional shear will be used below referring to the turning of the *wind shear vector* with height. Figure 1.1 shows examples for idealized hodographs. Note that for hodograph **A** neither the wind velocity vector nor the wind shear vector change direction with height while in hodograph **A'** the wind velocity vector turns clockwise with height but the wind shear vector does not turn at all. Both of these hodographs are characterized by unidirectional shear. The hodographs **B** and **B'** are characterized by a wind velocity vector and a wind shear vector both turning with height. Such an idealized hodograph is also referred to as half circle shear. The wind shear vectors of **B** and **B'** are identical but their wind velocity vectors are not.
Markowski and Richardson (2006) also emphasize that in the absence of surface drag the evolution of a simulated storm does only depend on the shape and length of the hodograph but not on its orientation or position relative to the origin. It is important to add that this is only true over flat terrain. Over complex terrain the wind is stronly influenced by the terrain itself.

1.3 Different Types of Convective Storms

The most basic and simple form of a convective storm is a short-lived single convective cell. It consists of a single updraft, which moves with the mean environmental wind. Condensation occurs directly within the updraft in the center of the cloud where hydrometeors start forming. When they have gained enough mass, they fall down into the updraft and eventually reach unsaturated air. As they start evaporating, the surrounding air cools due to the conversion of sensible heat into latent heat and the density increases. This process slows down the updraft until a large column of cold air loaded with rain water starts sinking through the updraft. As it reaches the ground it spreads and replaces the warm moist air, cutting off the cell's supply. This process usually dissipates the cell within about 30 minutes. Such storms are therefore hardly a severe threat. Even in the presence of high CAPE, such cells have a relatively short lifecycle.
It has been speculated since the early 20^{th} century that the change of the environmental wind with height is a necessary condition for the evolution of convective storms which are more complex and often more severe than the single cell storm described above. However, it took several decades until the dynamics of such systems was fully understood.
The formation of multicell storms depends on a balance between wind shear and CAPE. Multicell storms are often the result of mesoscale or even synoptic scale forcing such as cold fronts or drylines (boundaries between moist and heavier, dry air). This causes the cells to be grouped along a line which is called a squall line. It was shown by Rotunno et al. (1988) that if the shear-containing layer is shallow enough and the wind shear vector is oriented perpendicular to the squall line, the conditions favour the formation of new

updrafts along the moving edge of the cold pool, which is called gust front. However, if the shear layer is deep enough and the shear vector is not oriented perpendicular to the squall line, quasi-steady supercells tend to form along the squall line. Even if not triggered along a line, such conditions cause single initial cells to evolve into organized lines which sustain themselves by providing upward lifting along the gust front. Clockwise (counterclockwise) rotation of the wind shear vector with height supports supercellular development at the right (left) flank of squall lines.
Long lived supercells are rotating convective cells which are sustained by a separation of updraft and downdraft in the lower troposphere. They can only exist in environments with vertical wind shear. The vertical vorticity within the updraft is a result of the tilting of horizontal shearing vorticity into the vertical by a gradient of the vertical wind speed along the horizontal vortex tubes. This process is illustrated in Fig. 3.1a and b.

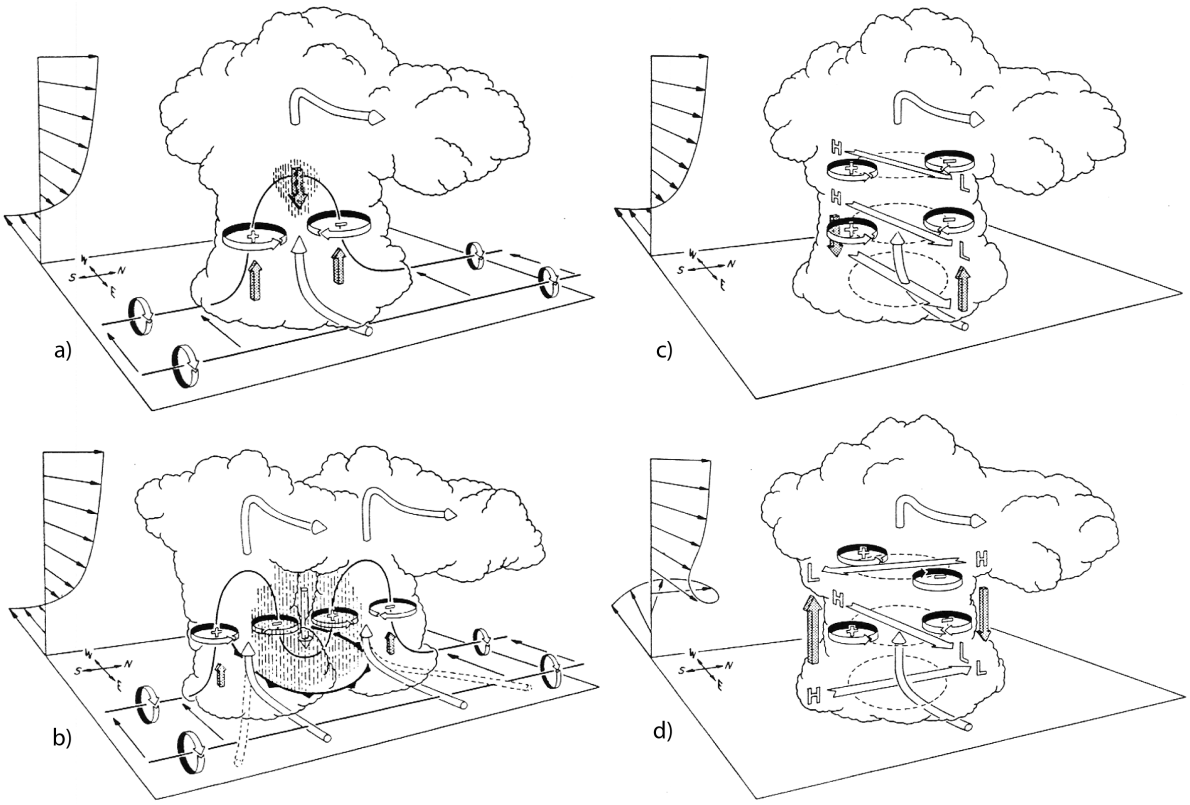

Figure 1.2: Schematic visualization of the splitting process (a and b) and the influence of a turning shear vector (c and d) on an updraft. The figure shows storm relative winds (bold white arrows) and vortex lines (thin black lines). The hatched area indicates rain water which is responsible for water loading and the splitting process in b. The grey bold arrows in c and d show the dynamic pressure gradient. Adapted from Klemp (1987).

Just like in a short-lived single cell, the center of the updraft weakens due to water loading and evaporative cooling. As a result, the updraft is split into two rotating updrafts. The rotation ensures that updraft and downdraft remain separated. The downdraft deposits cold air and precipitation to the left and behind the storm relative to its motion vector. These two downdraft centers are called front flank downdraft (FFD) and rear flank down-

draft (RFD), respectively. The updraft is fed by warm air approaching from the front right with respect to the storm motion. The system evolves into a rotating mesocyclone with the boundaries between warm and cold low level air masses assuming properties of warm (cold) fronts ahead (to the right) of the storm. This system can even show signs of occlusion. If a tornado forms it is located at the occlusion point of the mesocyclone. The formation and lifetime of tornadoes depends on a delicate balance between the warm and cold airmasses in the center of the low level vortex.
The occurrence of mixed forms, such as squall lines with supercellular development along their flanks, led to the conclusion that single cells and supercells should be viewed as building blocks which make up organized convective systems. The presence of vertical wind shear was identified as a necessary condition for the formation of organized convective systems. However, it has been shown that the shear profile alone is not sufficient to predict what kind of system will evolve in case of triggering. Weisman and Klemp (1982) could show that different shear profiles combined with different values of CAPE can lead to almost identical systems with different intensities. Higher CAPE values required a higher amount of unidirectional shear to support the same type of convective storm with higher intensity. Too much shear disturbed the updraft by shearing it apart and low shear coupled with high CAPE prevented the seperation of updraft and downdraft in the lower levels, resulting in storms whose cold pools cut of the supply of warm moist air.

1.4 The Simulation of Convective Storms

Convective storms have always been considered a great challenge for forecasters around the world. The development of high resolution mesoscale forecasting models has improved the predictability of severe storms. However, compared to synoptic scale phenomena a high degree of uncertainty remains.
The resolution of current operational global models is insufficient to accurately simulate deep moist convection. Even mesoscale models with convection permitting resolutions of 2 - 5 km fail at reproducing anything but the crudest storm scale circulation. Bryan et al. (2003) showed that the horizontal resolution necessary to simulate deep moist convection accurately is lower than $\mathcal{O}(100$ m). They simulated an idealized squall line to test the sensitivity of the storm to changes of the horizontal resolutions from 1 km down to 125 m. It turned out that even the mode of convection can change as a result of using a higher horizontal resolution. Whereas the 1 km simulations with weak shear produced a series of vertically oriented convective towers behind the gust front, in the 125 m simulations those changed into tilted moving plumes of rising air. Bryan et al. (2003) argued that the simulation of convective storms at resolutions of $\mathcal{O}(1$ km) is acceptable for operational purposes while higher resolutions of $\mathcal{O}(100$ m) should be used when studying a storm in detail. However, using 125 m resolution on large domains with several hundred kilometers in size is in present only possible on large supercomputers. Increasing the resolution from

1 km to 125 m increases the amount of memory required by a factor of 64 and the amount of calculations required by a factor of 512. These numbers are even higher if vertical resolution is increased or more complex physics and subgrid turbulence parameterization schemes are used.
Simulated storms are not only sensitive to horizontal resolution. Adlerman and Droegemeier (2002) have shown that a simulated storm can be very sensitive to several model parameters. They simulated a storm and examined the occurence of cyclic mesocyclogenesis (the formation of a new low level vorticity maximum after the occlusion of the mesocyclone). The duration of the cycle showed a strong sensitivity to horizontal and vertical resolution as well as to the model's physical settings such as microphysics, numerical diffusion and friction. These results might seem rather discouraging. Nevertheless, simulations have provided very valuable insight into storm dynamics over the last decades. The scale at which convective storms are triggered can be well beyond the resolution of any weather forecasting model. In the presence of strong instability - especially if coupled with low CIN values - even small rising parcels of warm air over convergence zones or small scale orographic obstacles can theoretically initiate a severe storm. Since it is impossible to accurately capture such phenomena in operational forecasting models, the triggering process is very difficult to handle in such simulations.

1.5 Early Modeling Studies

Schlesinger (1973) was one of the first to run simulations of deep moist convection involving vertical wind shear. His simulations were 2-D and showed that with increasing vertical wind shear the updraft intensity decreases while its duration increases. He assumed correctly that 2-D simulations are not capable of reproducing certain mechanisms that influence storm development in 3-D sheared environments.
The early publications using three dimensional cloud resolving models also date back to the early 1970s. One of the first papers on the 3-D simulation of a thunderstorm was by Wilhelmson (1974). His results indicate that the 3-D storm is more intense than previously modeled 2-D storms. The air flow around the updraft at mid levels showed features similar to a flow around a cylindrical obstacle. A dynamic vertical pressure gradient developed which decelerated the updraft. Later, Klemp and Wilhelmson (1978) showed that in unsheared environments the convection is dissipated by water loading while sheared environments favour updraft splitting and lead to a vortex couplet, along with a longer life cycle and the triggering of secondary convection. Splitting updrafts form two separate rotating storm cells which move to the right and left relative to the environmental mean wind. Such split storms have been observed in nature, the right moving storm (RMS) is often stronger and longer lived than the left moving storm (LMS). (See for example Bunkers (2002)).

The influence of directional shear on a storm was first fully described by Rotunno and Klemp (1982). They conducted simulations using a hodograph measured near Del City, Oklahoma in 1977 during a severe storm event and an idealized straight line hodograph which contained about the same magnitude of shear below 6 km. Their results showed that the straight line hodograph caused the initial updraft to develop into a symmetric split storm while the clockwise curved hodograph caused the RMS to be dominant. They used the cylinder flow analogy to derive a linear theory which describes the dynamical vertical pressure gradient in the evolving updraft. Using that theory they showed that only in the presence of directional shear can one of the split storms develop faster and stronger than its counterpart. Clockwise curvature of the hodograph supports a dominant RMS while counterclockwise curvature supports a dominant LMS.
Weisman and Klemp (1982) conducted a variety of simulations covering a 2-D parameter space defined by a range of vertical wind shear and CAPE values. Even without including directional shear, boundary-layer processes and ice microphysics in their model, they were able to reproduce a spectrum of convective storms ranging from short-lived single cells to multicells and to splitting supercell storms also observed in nature. These tests confirmed the assumption that CAPE and shear are two very important parameters for the evolution of convective systems.
Later tests by Weisman and Klemp (1984) included a variety of vertical wind profiles with directional shear. Their hodographs turned clockwise in the lowest 5 km and the wind above was kept constant. The shape of the hodographs was identical to that of **B** and **B'** shown in Fig. 1.1, this kind of profile is also referred to as half circle shear. The radius of the half circle was varied to produce different magnitudes of shear. Just like with the straight hodographs Weisman and Klemp (1984) were able to reproduce single cells, multicells and supercells for low, moderate and high shear, respectively. When supercells and multicells were present, the supercells were found only on the right bank of the storm system while multicells were confined to the left bank. For counterclockwise shear the development is inverse.

1.6 Idealized Modeling Studies on the Interaction with Terrain

Frame and Markowski (2006) simulated a squall line moving over an idealized ridge. In all their simulations the squall line moved perpendicular to a mountain ridge. The tests included different mountain widths and heights and found that higher mountains as well as wider mountains both produce a stronger precipitation maximum on the windward side and a minimum on the lee side of the ridge.
One of the difficulties of idealized simulations over mountains is demonstrated in Reeves and Lin (2007), who also tested the effects of a mountain ridge on a pre-existing squall

line. In their simulations, a second convective system is triggered by the mountain ridge and then influenced by the environmental wind. The effects of the triggered and preexisting convective systems interfere with each other. To distinguish the effects of these systems, Reeves and Lin (2007) conducted a series of control simulations either without the preexisting system or without the mountain ridge. Their simulations showed that for low environmental wind both convective systems travel upstream. Stronger environmental winds advect the cold pools, which form below the convective cell, downstream and thereby inhibit upstream propagation. Instead, simulations with higher wind speed showed stationary storms upstream of the mountains which were maintained by cold pools along the upstream side of the mountains, which were the result of evaporative cooling beneath the convective cells.
One of the most recent approaches is by Markowski and Dotzek (2011). Their simulations contained a right moving supercell storm in a quarter circle shear environment moving over different shapes of 500 m tall idealized 2-D and 3-D terrains. The usage of a slightly drier sounding than the one used by Weisman and Klemp (1982) and a rather low mountain prevented triggering by orographic lifting. Their tests with 2-D and 3-D terrain showed that supercells tend to adjust to changes in the environmental thermodynamic and wind fields caused by flow over or around topography. Changes in CIN and CAPE seem to have the strongest effect on the moving supercells. While the magnitude of changes in CIN and CAPE were similar with $\mathcal{O}(100)$ J kg^{-1} K^{-1}, the relative change was very different. CAPE varied by only about 10% while CIN varied by over 50% of its initial value depending on the location relative to the mountain ridge. Horizontal variations in the vertical vorticity field were present when using 3-D terrain. While they had an effect on the low level rotation of the supercells, their overall effect on the supercells was described to be relatively low.

1.7 Real Case Simulations

While idealized simulations can be initialized with very simple conditions that can easily be modified, they ignore a large number of possible factors that influence real storms. For a long time it was computationally too expensive to simulate even a small nested domain on a convection resolving scale. Nowadays such models are developing very fast and many national weather services run their own nested models to predict the occurence of severe convective events. In fact a very basic convective forecast can even be done on a last generation personal computer today.
Real terrain is never perfectly flat. While the current horizontal resolutions of 3 to 5 km are sufficiently fine to capture mesoscale convective systems over relatively flat terrain, e.g. the Great Plains, such resolutions are not sufficient to model the interactions between complex terrain and the atmosphere. One possible approach is to use very high resolution models. However, increasing the resoultion also increases the hardware requirements

drastically and does not guarantee successful modeling of convective storms. Therefore, it is not feasible for operational purposes. Using very low grid spacing with $\mathcal{O}(1\text{ km})$ or even less is becoming increasingly common in reasearch simulations, where fast simulations are not as important as in operational forecasts.

1.7.1 The Papal Front

"The Papal Front of 3 May 1987 was named as such because it disrupted the helicopter flight which was to take the Pope from Munich to Augsburg" (Sherwood, 1995). The Papal Front is an extraordinary example of rapid and severe cold front development north of the Alps. The cold front developed squall-line-like character and produced a series of thunderstorms and strong winds. The Papal Front is not only a very interesting case, but it has also been documented and analyzed in detail. Although the operational models were not capable of capturing squall lines back in 1995, this can be considered one of the early real case studies which dealt with a convective system. Sherwood (1995) looked at the case from a forecaster's perspective and concluded that the initial release of conditional instability was caused by forced rising motion along the Alps. The release of conditional instability then triggered a positive feedback loop which caused intense isallobaric winds due to rapid pressure rises beneath the cold air. The cold advection aloft contributed to the destabilization. The weather was much less severe once the front was further east and farther away from the Alps.
Volkert et al. (1995) simulated the front using several operational weather models available at the time. The goal was to find out to what extent the operational models are able to capture the severe development. Considering the models' resolutions of 17 - 90 km in 1995, a mesoscale convective system still posed a challenge for forecasters and models. While the intensification of the front was captured by the models it was underestimated. The orographic jet along the Alps, which formed due to air being forced around the ridge, was well modeled and the precipitation parameterization predicted (convective) precipitation of the same magnitude as observed. The convective system itself was not simulated since 17 km is much too coarse to capture a squall line and convection had to be parameterized. Volkert and Steinacker (1995) did a research-type analysis and concluded that the knowledge of upper air fields is essential to forecasters to predict the development of convective storms.

1.7.2 The Predictability of an Isolated Thunderstorm

One of the very recent approaches to modeling of real cases was that of Hanley et al. (2011). They ran the model 24 times with slightly variing initial conditions (ensemble) to test the predictability of an isolated thunderstorm over the Black Forest in Germany. Due to the stochastic nature of the planetary boundary layer the use of ensembles is a logical

choice. Hanley et al. (2011) found that the ensemble failed to predict deep convection entirely unless the moisture contents of the soil was increased by 25% and the specific humidity q_v in the lowest 1 km of the atmosphere was increased by 3 g kg^{-1}. However, even after applying these corrections only some of the ensemble members produced deep convection at all. Twelve members modeled convection with cloud tops of less than 4 km altitude while 4 members modeled cloud tops of over 12 km and in 3 of them the location was off by less than 50 km. Hanley et al. (2011) concluded that the large differences throughout the ensemble members resulted from conditions which were barely sufficient to trigger deep convection. These results are of particular interest for this work since they were obtained using the same model and a similar resolution (1000 m vs. 833.33 m) as it is used in the course of the simulations described in the chapters below.

1.8 Convective Potential in the Alpine Region

Ortner (2008) has done a detailed analysis of the CAPE values measured at weather stations in the Alpine region. For this purpose he analyzed CAPE reports from 11 stations in the time period from 1980 to 2006. His results show that CAPE values in the Alps rarely exceed 2000 J kg^{-1}. One very important result is that most thunderstorms which were observed between 1980 and 2006 occurred while a CAPE of 500 J kg^{-1} or less was present. Krimml, as an example of a station located in a narrow Alpine valley, has only 9 reports of CAPE over 500 J kg^{-1} and less than 4% of all reports show CAPE > 0.

Chapter 2

Case Study of Severe Convection over the Alps

2.1 The Storm of 2 August 2007

This section contains a lot of geographical references. Appendix C contains a map showing both, real and simulated, storm paths and geographical references used in this chapter. On August 2 2007 a convective storm with supercellular development at its southern flank and multicellular features at its northern flank moved along the northern side of the Alps for more than eight hours. Given that supercells are an uncommon phenomenon in the Alps, this storm is of particular interest because of its longevity and the fact that it moved over several high mountain peaks exceeding 3000 m in height. The Zentralanstalt für Meteorologie und Geodynamik (ZAMG) in Vienna has a short reference to the date of the storm in their archive:

> "Am 2. entstehen entlang der Linie Wattens in Tirol - Schladming im Ennstal schwere Nässe- und Hagelschäden. In Tirol stehen im Gemeindegebiet von Wattens und in Kaltenbach im Zillertal zahlreiche Keller unter Wasser. Mit den Regen gehen golfballgroße Hagelschlossen nieder. In Salzburg wird im Pinzgau während des Hagelschlages in Kaprun ein Hoteldach vom Sturm teilweise abgedeckt. In der Gemeinde Piesendorf liegen die Hagelkörner bis zu 25 cm hoch. Fluren stehen teilweise unter Wasser, ebenso in Zell am See. Nahe Radstadt werden sieben Schüler bei einer Wanderung von den Hagelschlossen verletzt. In weiterer Folge entstehen Schäden in der Obersteiermark, mit schweren Hagelschlägen im Bereich von Schladming und Haus im Ennstal und Starkregen bis in den Raum Liezen. Die landwirtschaftlichen Hagelschäden in Tirol und in Salzburg werden auf mehr als 650.000 EURO geschätzt." (ZAMG, 2007)

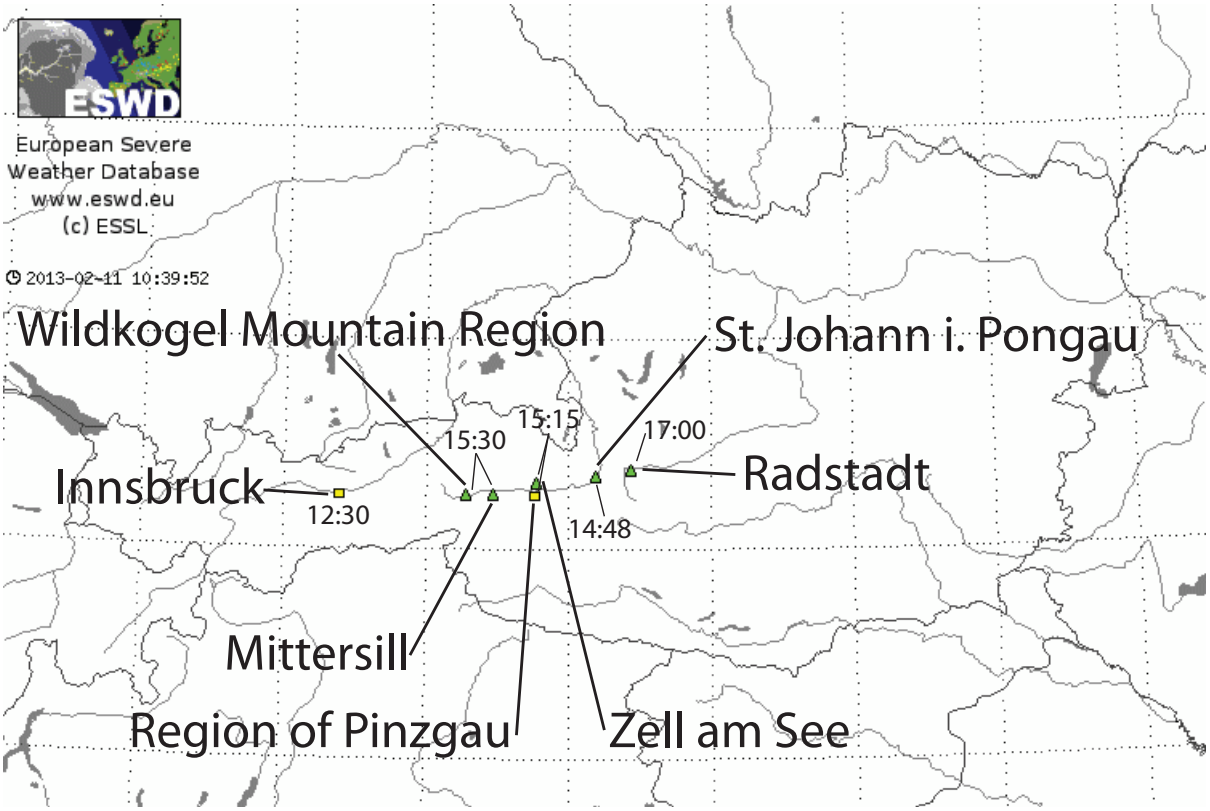

Figure 2.1: ESWD entries for 2007-08-02 between 10 and 19 UTC. The green triangles indicate large hail and the yellow squares mark locations of severe wind reports. The times are given with an error interval of 1 hour. (Image courtesy of ESSL, adapted by the author).

The above-mentioned line between Wattens and Schladming is the section of the supercell's path where it reached its highest intensity according to radar imagery, exceeding 60 dBz. During this phase the cell produced large amounts of hail with grain sizes reaching several centimeters in diameter and very high precipitation rates.

The European Severe Storms Laboratory (ESSL) maintains the European Severe Weather Database (ESWD), where severe weather events are documented and archived. The ESWD data regarding the storm of August 2 includes five reports of large hail and two reports of severe winds. The data is based on local news and eyewitness reports. The alignment of all reports along a line following the Inn and Salzach rivers is striking. The storm track reconstruction by Jaeneke (2007) shown below in Fig. 2.4 indicates that the storm passed over this area during its phase of highest intensity. The severe winds in Innsbruck were reported at 12:50 UTC, the events from the Wildkogel region to St. Johann im Pongau were reported between 14:48 and 15:30. There is a large hail report for Radstadt at 17 UTC. The possible error interval given by the ESWD is 1 hour for all reports. Theoretically, this allows a continuous motion of the convective system from the west to the east.

A more detailed analysis was done by Jaeneke (2007) from the Deutscher Wetterdienst (DWD). The analysis is freely accessible from the website Unwetterstatistik Österreich. The cell was tracked from eastern Switzerland via Tyrol and Salzburg to Lower Austria by using radar imagery. The surface analysis in Fig. 2.2 shows the synoptic conditions during the night before the thunderstorms occurred. The situation on August 2 2007 was characterized by a strong surface low over the North Sea with a weaker surface low over central France northeast. Its cold front approached the Alps from the northwest and already caused strong convective storms over France during the night.

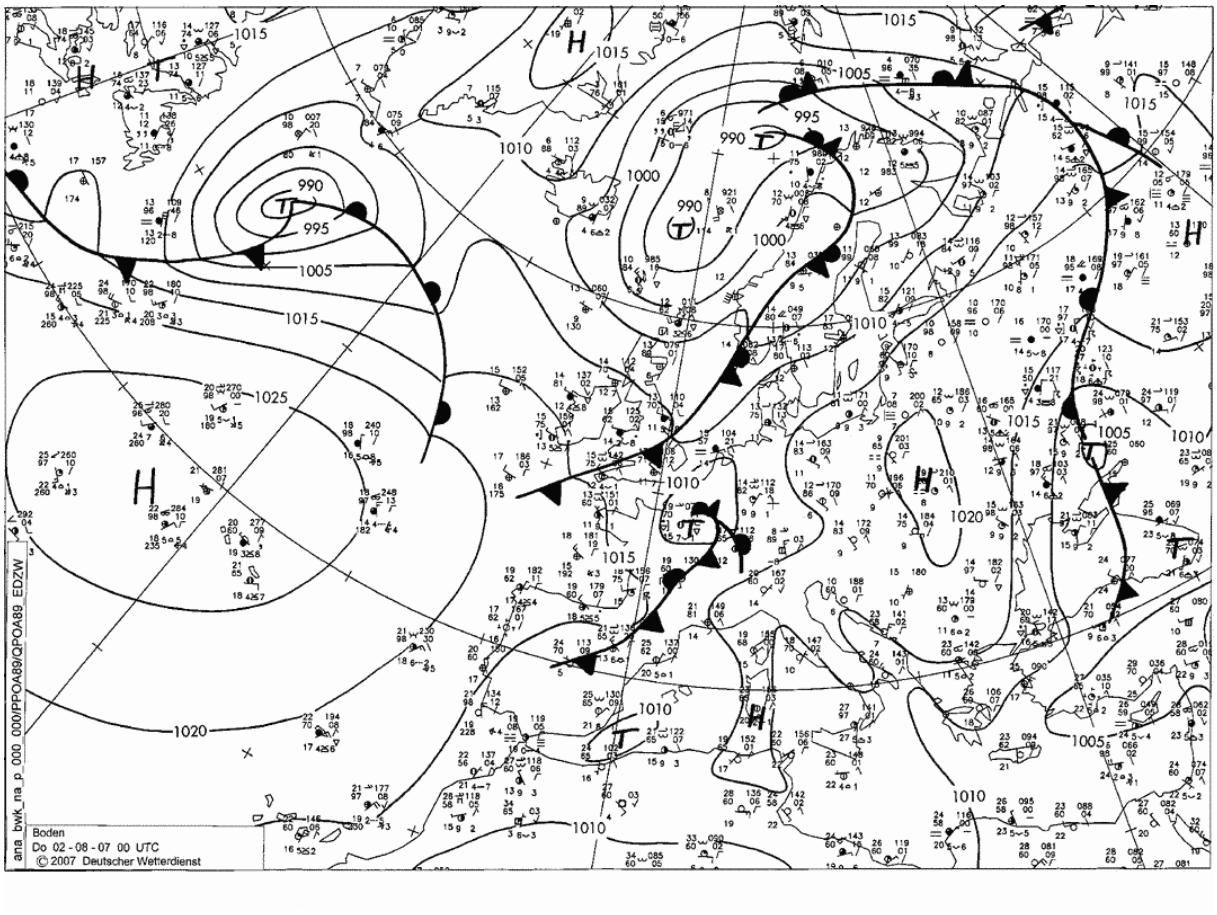

Figure 2.2: DWD surface analysis 2007-08-02 00 UTC

Both the 1000 hPa to 500 hPa thickness and θ_e shown in the reanalysis in Fig. 2.3 indicate very warm air masses in the Alpine region, while the cold front was still north of the Alps. The front is represented by a strong gradient of θ_e over southeastern France. However, the surface front is ahead of the frontal zone in 850 hPa due to its tilt with height. At 12 UTC the cold air masses had already approached the Alps and caused several storm cells over Switzerland along the northern Alps and over western Austria.

The super-multicell showed up on the radar shortly before 10:00 UTC about 10 km southwest of Davos in eastern Switzerland. It moved rapidly through the Engadin towards

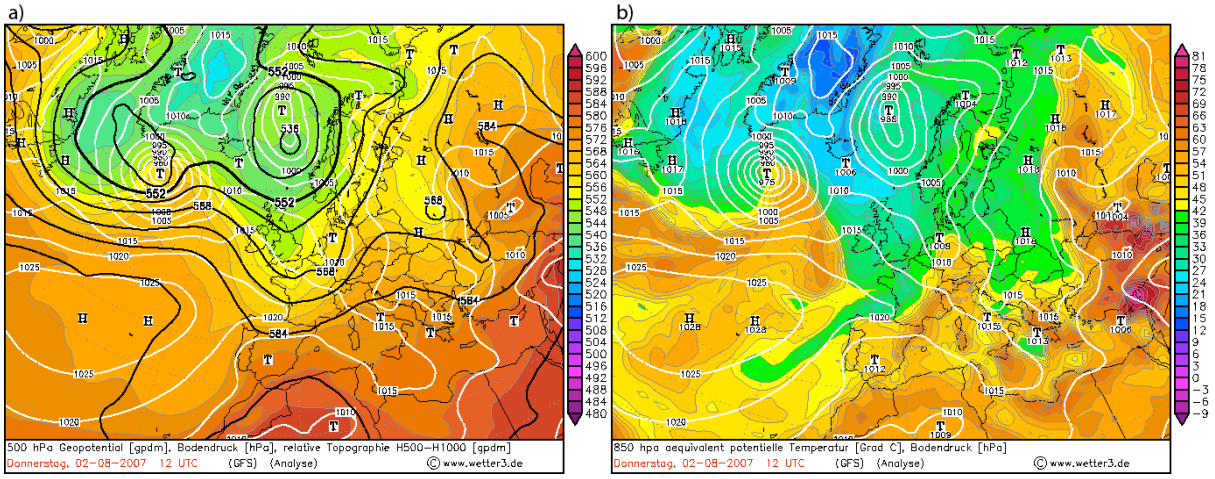

Figure 2.3: Reanalysis for 2007-08-02 12 UTC showing plots of the (a) 500 hPa Geopotential (contour lines), 1000 to 500 hPa thickness (color) and (b) 850 hPa pseudopotential temperature. The white lines show the surface pressure field. (www.wetter3.de)

Ischgl in Tyrol, following the Inn towards east-northeast. Before reaching Innsbruck it started moving almost parallel to the Inn valley over the Ötztal Alps and entered it again at 12:30 UTC, hitting Innsbruck.

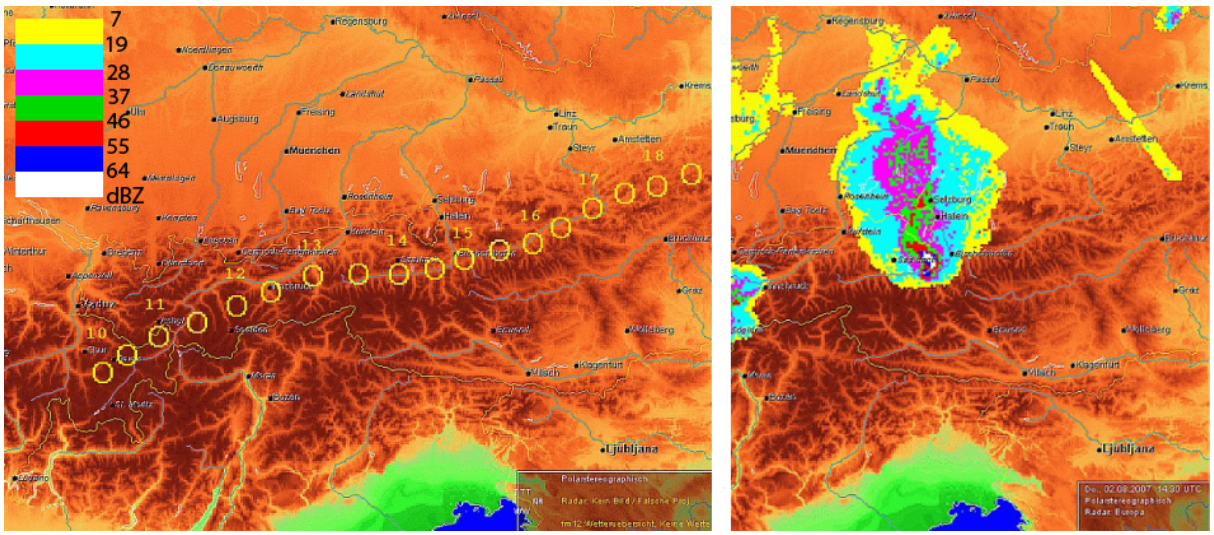

Figure 2.4: Left: Location of the cells updraft core according to maximum reflectivity. Right: Example for radar image. From Jaeneke (2007)

Right after moving along the relatively wide Inn Valley the storm intensified, reaching reflectivity values of about 59 dBz while moving on towards Salzburg over the Tuxer Alps into the Salzach Valley. This was the cell's most active phase with reflectivity values exceeding 60 dBz on the Munich weather radar. During this period the cell produced extreme hail which accumulated up to 25 cm in Piesendorf according to the ZAMG. However, it is not mentioned whether this is an accumulated value for a certain area or the height of the hail layer at certain points where the grains gathered due to terrain slopes

or along obstacles. In any case, this amount of hail is uncommon in the Alpine valleys and potentially very destructive. The path then followed the Salzach valley and the Enns valley and ended in the area of Rax where it dissipated around 18:30 UTC.
The cell traveled a total distance of over 420 km within less than 9 hours. While most of the thunderstorms in the Alpine region occur either in the northern or southern foothills, this storm moved along the main ridge over relatively high terrain. It moved along or parallel to relatively wide valleys where one would assume a better supply of warm moist air.

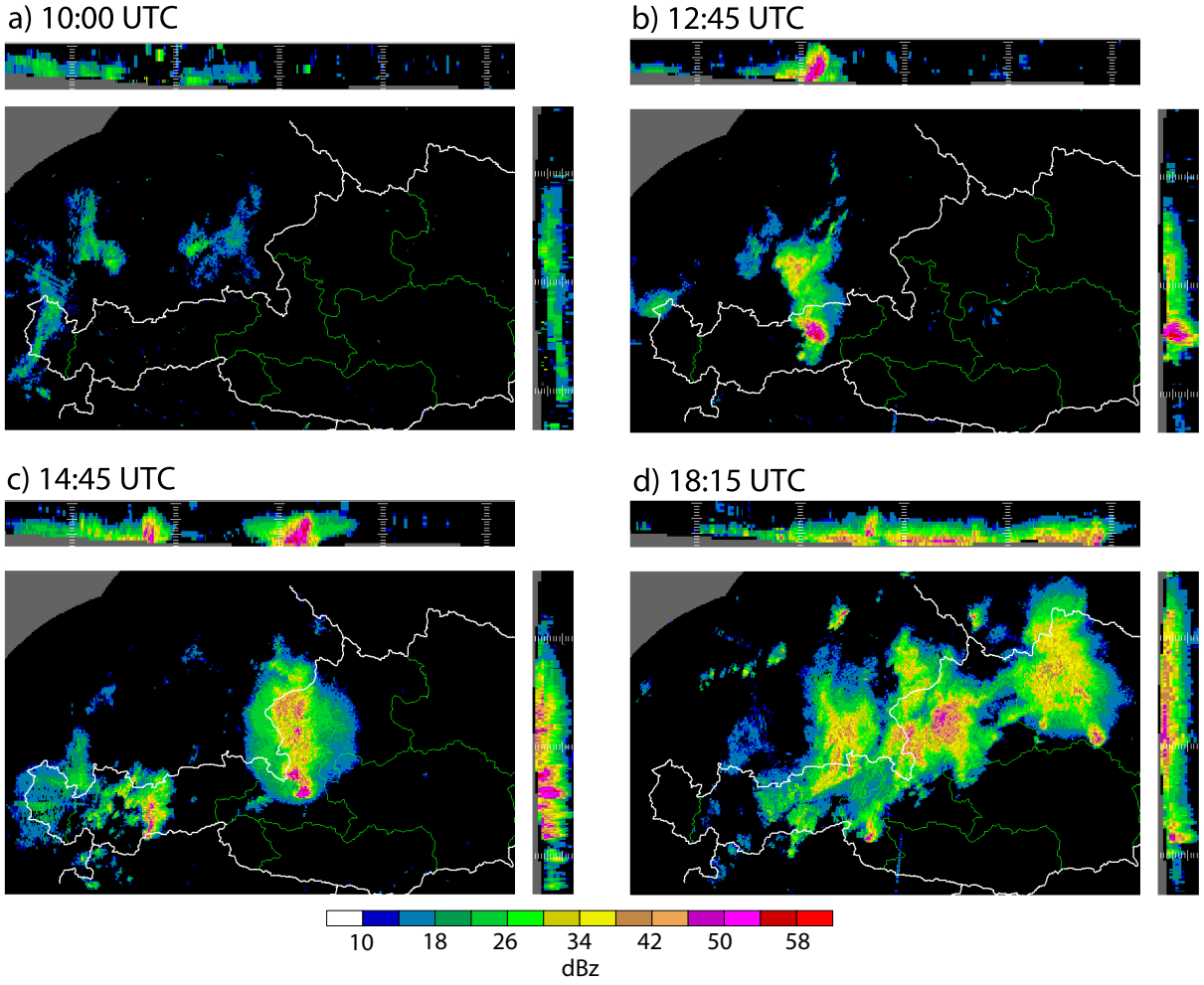

Figure 2.5: Radar images from 2007-08-02 for four time steps. The reflectivity maximum for each vertical column is shown in the large panels. The smaller horizontal (vertical) panels show the maximum reflectivity for each horizontal north-south (east-weast) row. The white long (short) dashes indicate the height in steps of 5000 (1000) mASL. (© Austro Control)

Figure 2.5 shows a series of four radar images from the Austrian weather radar, which is run by the Austro Control. Figure 2.5a shows the first sign of the supercell at 10 UTC over Switzerland. It is marked in the lower left corner of the image. Signs of weaker convective precipitation over Vorarlberg and southern Germany is visible in the same figure at 10

UTC. The development into a convective line is shown in Fig. 2.5b. The pink and red core of the supercell is clearly visible and a secondary maximum shows over Bavaria in orange and pink. The multicellular character of the system north of the supercell becomes even better visible at 14:45 UTC in Fig. 2.5c, where an intense second maximum with similar reflectivity values as the supercell's core is visible over the border between Austria and Germany, close to the city of Salzburg. A second system with high reflectivity values and a convective line is visible over western Tyrol. As apparent in Fig. 2.5d, a third system develops behind the two which are visible in Fig. 2.5c. At 18:15 UTC the supercell's updraft is still visible in pink over the border between Styria and Lower Austria. This is the last time step with such a clear signal of the supercell. The system quickly decays after 18:15 UTC.

Figure 2.6 shows the area where the storm was triggered shortly before and after its initiation. The likely reason for the triggering is a combination of orographically induced convergence along with cold pool induced convergence. Below it will be shown that the model storm was most likely initiated by those mechanisms.

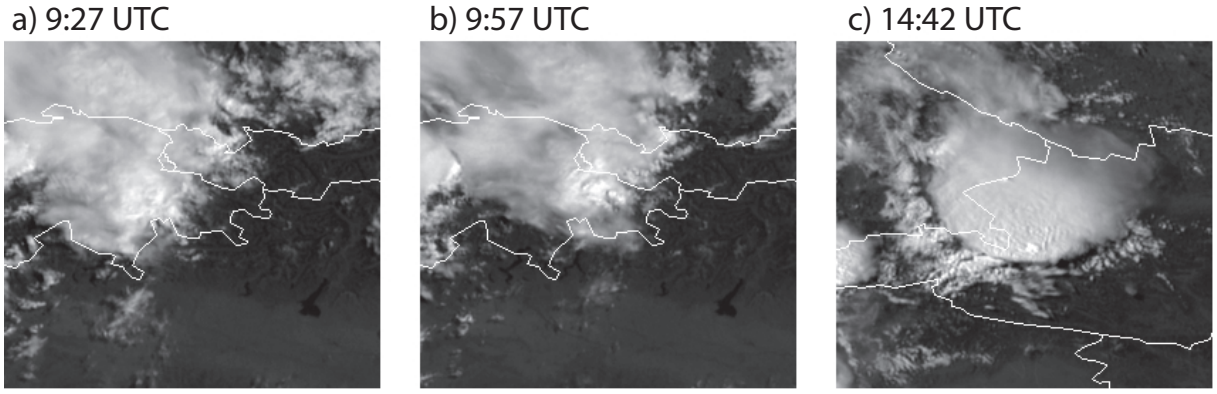

Figure 2.6: High resolution visible satellite images of the initiation (a, b) and mature (c) supercell stages. (© ZAMG)

Even though it would have been desirable, there are no radio sounings available which show any significant CAPE in the vincinity of this interesting event. Munich and Vienna, where two soundings each day (00 UTC and 12 UTC) are available, are too far from the storm track and did not register any CAPE value higher than 50 J kg^{-1}. Both, Innsbruck and Linz, are much closer to the storm's track. However, their soundings are done at 3 UTC. At this time no CAPE was measured.

Figure 2.7 shows the skew-t diagram for Munich at 12 UTC. The CAPE given at this time is 40 J kg^{-1} K^{-1}. The air directly above the ground is very dry with the difference between T and T_d reaching over 12 K. While q_v is almost 10 g kg^{-1} directly above the surface it is lower within the mixed layer, which shows values of about 8 g kg^{-1}. Along with the strong overadiabatic temperature gradient directly over the surface, this indicates upward flux of latent and sensible heat from to soil into the atmosphere.

It is also apparent that the CAPE is not calculated from the surface values, which would

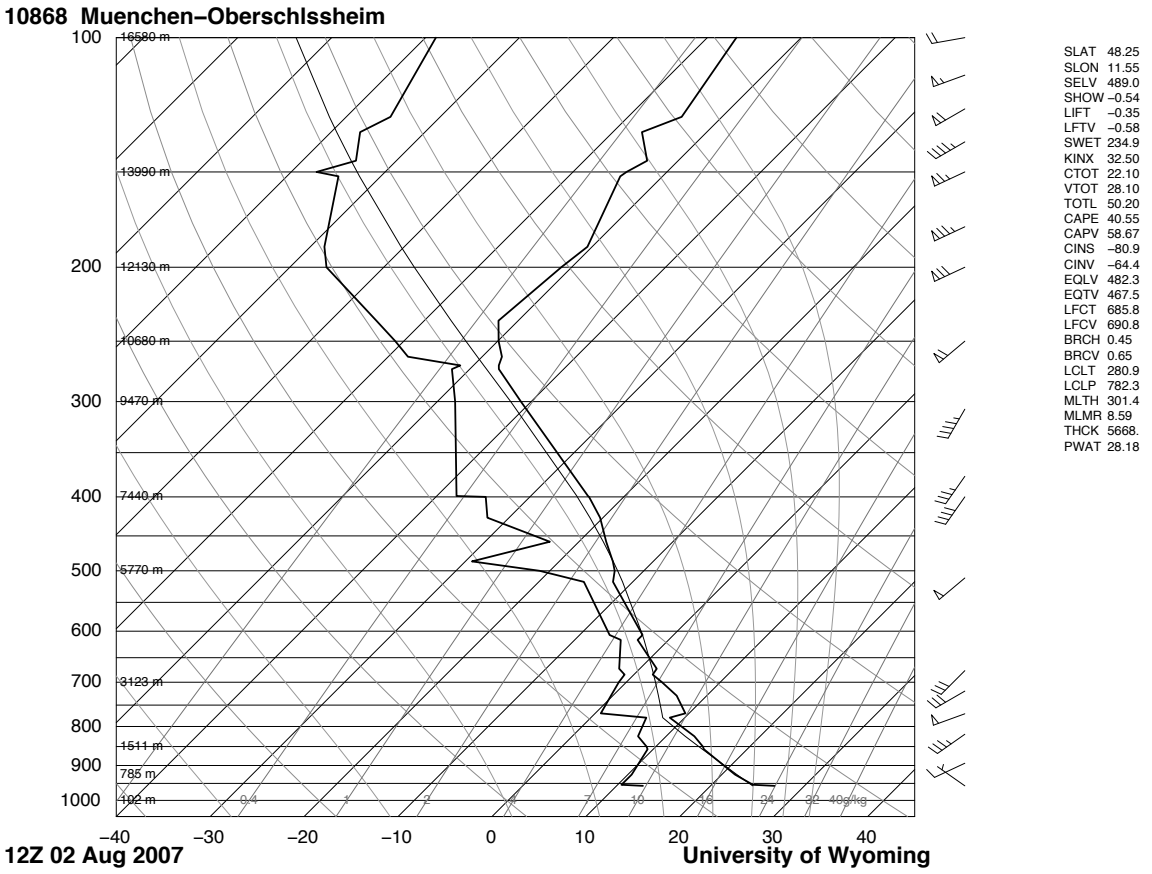

Figure 2.7: Skew-T log-p diagram for Munich at 2007-08-02 12 UTC. The x-axis shows T [K], the y-axis pressure in logarithmic scale. The bold black lines tilted to the right with height are isotherms, the thin lines tilted to the right are lines of constant specific humidity q_v [g kg^{-1}] water vapor per kg of moist air. The curved thing grey lines mark lines of constant θ_e^*. (Image by the University University of Wyoming (2013))

yield a much higher result due to T and T_d being about 2 K higher than in the mixed layer. The wind barbs to the right show a strong vertical wind shear between 950 and 850 hPa.

2.2 Numerical Model Setup for the Real Case Simulation

The WRF model was used to simulate the convective storm event of 2 August 2007. The setup consists of three domains. The outermost Domain 1 has a horizontal grid spacing of 12.5 km. It covers most of Europe and guarantees good coverage of the region where the large scale low pressure system, which builds up the conditions for the convective storms, is located. Domain 2 has a horizontal grid spacing of 2.5 km and covers the Alpine region up to central Germany and France to capture the northwesterly advection and frontal zones. The innermost, Domain 3, is located directly over the Alps and covers most of the

main Alpine ridge within Austria and the Alps' northern foothills as well as the north of Switzerland. Its horizontal grid spacing is 833.33 m. Figure 2.8 shows a contour plot of the model terrain. The time steps for these domains are 75, 15 and 5 s, respectively.
The map is on a Lambert conformal projection with the reference longitude being chosen at 28° East to obtain a slight clockwise rotation of the domain. This aligns the x-axis parallel to the real storm track and allows a relatively narrow Domain 3. As a result the reference longitude is off the map in eastern direction. The reference latitudes are 30° and 60° respectively.
In all domains there are 61 vertical levels, which are arranged automatically by WRF. The model uses terrain-following η-coordinates. The resolution is highest directly over the ground and along the assumed top of the planetary boundary layer between . The highest layer is located at 5000 Pa (roughly 21000 m) and is a rigid lid. A 5000 m thick Rayleigh damping layer is placed below the model top.
The microphysics is handled by the Goddard GCE scheme. This scheme was used in the simulations of Markowski and Dotzek (2011). It includes cloud water, cloud ice, rain, snow and graupel. Cumulus parameterization is only used in the two outer domains, where the Kain-Fritsch scheme is . The radiation is handled by the RRTM scheme (long wave) and Dudhia scheme (short wave) and is calculated every two minutes.

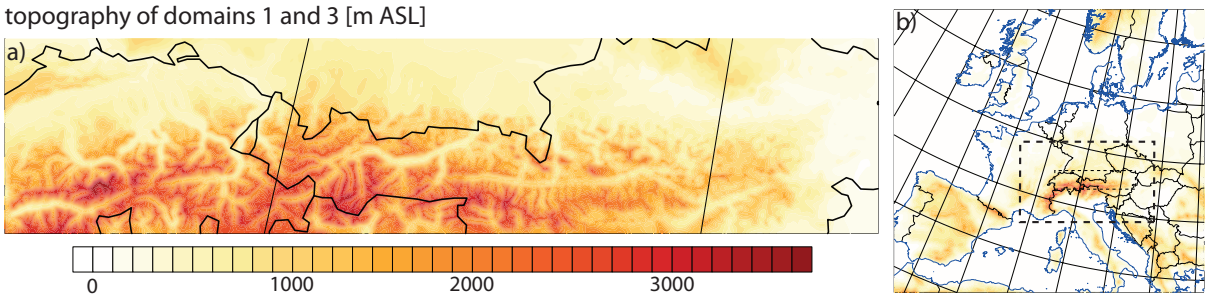

Figure 2.8: Contour plot of the model topography. Domain 3 is shown enlarged in (a) for better visibility. Domains 2 and 3 are indicated by the large and small dashed rectangles in (b).

2.3 Results

At a first glance the simulations resemble the documented storm event very well. A convective system is produced which moves directly north of the main crest of the Alps and has its most intense phase while it travels over the east of Tyrol and over Salzburg. However, there are some important differences. The simulated storm originates farther east, where it is triggered over the Lechatal Alps. The triggering spot is also farther north than shown in the radar images shown in 2.5. The storm then moves along the Inn valley. A second system is initiated farther southwest and travels at a greater speed, eventually

catching up to the initial convective storm.

2.3.1 The Prestorm Conditions

The model's surface pressure field, shown in Fig. 2.9 d-f, is harder to interpret than the reanalysis in Fig. 2.2. The reason is that the model resolves a certain degree of convection even in domain 2 which leads to the evolution of updrafts and cold pools. Those have a significant impact on the mesoscale structure of the surface pressure field. The topography is better represented in higher resolution simulations, namely domain 2 and domain 3, which also causes a strong signal in the surface pressure. For that reason the field is not shown at grid points where the topography is higher than 1000 m above sea level (ASL). This is a rather crude method, but it conserves the most important features of the field which are situated north of the Alps over relatively low and flat terrain.
Since the impact on the 850 hPa θ_e-field (Fig. 2.9 d-f) is less extreme the field shows the frontal zones well. Convection distorts the cold front signal over Switzerland and along the border between France and Germany just before it approaches the Alps. The surface cold (warm) front is ahead (behind) of the 850 hPa front due to the tilt of the frontal zone with height.

Figure 2.9 a-c show how the warm front moves eastward north of the Alps. In Fig. 2.9a the occlusion process is visible in the northwestern corner of the figure. A pocket of warm air along the northern side of the Alps is visible. The 850 hPa cold front signal is distorted by colder regions aligned along a northeasterly pointing line which are the result of convective storms. They occured over France during the night and can be seen in the simulation. In the model they produced precipitation maxima up to 42 mm within less than two hours. They distort the surface pressure field in 2.9d and the updrafts affect the 500 hPa topography. In 2.9b the surface warm front signal has moved towards the east and shows a strong gradient along a wavy line. The signal of the warm sector in the 850 hPa and surface θ_e fields is much weaker at 6 UTC, which is shown in Fig. 2.9b. This is caused by convective overturning. The surface warm sector air masses have a θ_e of about 330 K while the thunderstorms' cold pools are characterized by values of 320 - 322 K. They cover a relatively small area at 00 UTC but extend over large parts of Baden-Würtemberg and the Alsace at 6 UTC and have almost fully replaced the surface warm sector airmasses north of the Alps except in France along the border to Switzerland. At this time storm activity is at a minimum and there are no strong updrafts located in domain 2.
New updrafts start forming along the north of the Alps over Switzerland at around 7 UTC and intensify until 13 UTC, forming lines of convective cells oriented almost parallel to the Alps' main ridge. The most intense precipitation of up to 54 mm total occurs in the Valais along the Rhône valley. That area is located in the very west of domain 3 and its higher resolution makes local heavy precipitation more likely than in domain 2.

Shortly before 12 UTC an area of increased θ_e forms directly along the northside of the Alps in Tyrol and Salzburg with values exceeding 334 K at the surface and 330 K at 850 hPa. This region of warm air is associated with CAPE values of 800 to 1200 J kg^{-1}. These are rather moderate values for the observed severe weather. The values later during the day were of similar magnitude. In comparison, the thunderstorms over France during the night were associated with higher simulated CAPE in excess of 2100 J kg^{-1}. Between 6 UTC and 12 UTC the 500 hPa trough moves from France towards the Alpine region. The mid and high level winds turn southwest and increas in speed.
The comparison between θ and θ_e shows that the warm pocket has a much weaker signal in the potential temperature field than in the equivalent potential temperature field. This indicates that the rise in θ_e is mainly associated with an increase of latent heat. The water vapor mixing ratio q_v was examined and shows a similarly strong signal as θ_e, confirming that moisture is the reason for the high θ_e values. Looking at q_v reveals that a buildup of moisture along the northern flank of the Alps occurred just after 6 UTC, moving from the west to the east. Figure 2.10 shows how the moisture built up during the day, starting in Switzerland and moving further east over time. The darker areas show early concentration of moisture. Later consecutive time steps are brighter and placed behind the older contours to show the expansion of the moisture field. The darkest areas are mainly associated with lakes, with the patch in the very northwest of the domain being the exception. While in most areas the air was rather dry during the night, q_v never dropped below 10 g kg^{-1} over the lakes. The contours are filled to hide receding parts of the field since their retreat is mainly caused by the thunderstorm itself when warm moist air is replaced by colder air from the outflow. While the cold pool is a very important part of the storm's evolution - especially over complex terrain - it is not important for the buildup of moisture. The cold pool and its interaction with the topography will be discussed below. While Fig. 2.10 shows where and when the moisture increased above 10 g kg^{-1}, it does not explain its origin.

2.3.2 The Initiation

What caused the triggering in the model and why did it occur at a different location? Since an ensemble such as that used by Hanley et al. (2011) is not available in this case, the only possibility is to analyze the model output in detail. The initiation of the supercell storm is not the first convective event in Domain 3. Some convective cells occur at around 7 to 8 UTC over northwestern Switzerland but their development stops. However, they might play an important role in the initiation of the supercell via their cold pool. The cold anomaly, marked by the large ellipsis **A'** in the θ_e field in Fig. 2.12 is advected eastward and the convergence zone which is preceeding the cold air reaches the triggering area **A** in 2.12a around 10 UTC, only minutes before the model storm is initiated. The zone of the strongest θ_e-gradient directly ahead of the old cold pool follows the convergence zone. Convergence is also present at several other locations throughout the domain. The distri-

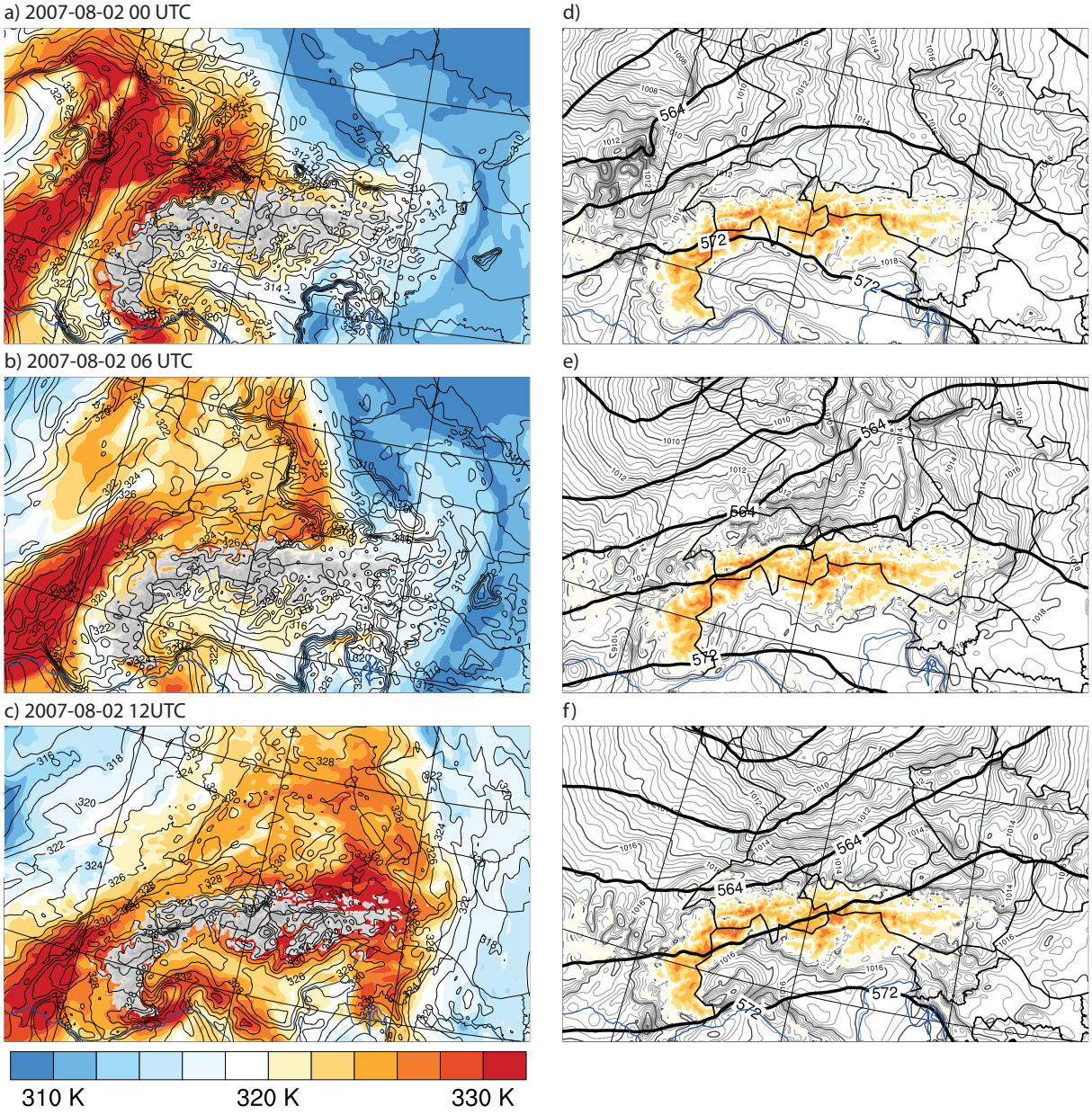

Figure 2.9: Prestorm conditions in Domain 2 every 6 hours starting at 2007-08-02 00 UTC: θ_e at 850 hPa (color) and in the lowest model level (solid thin lines) is shown in a, b and c with a contour spacing of 2 K. The terrain is shown in grayscale where it intersects and exceeds the 850 hPa pressure layer. The 500 hPa geopotential height is shown by the thick solid lines with an interval of 40 gpdm and the sea level pressure is shown by the thin black (and grey) solid lines with invervals of 1 (0.2) hPa in d, e and f. The sea level pressure is replaced by a colored terrain contour where the terrain height exceeds 1000 m above sea level due to unrealistic effects on the field.

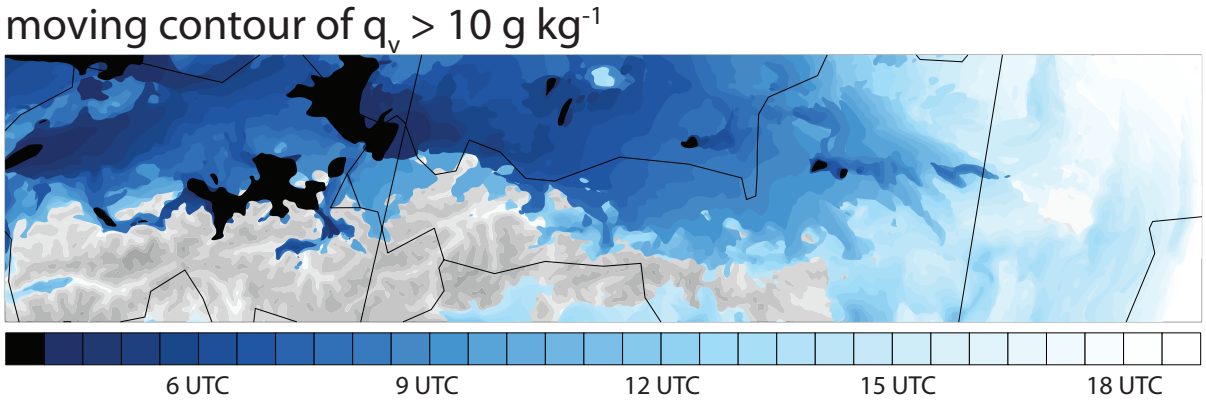

Figure 2.10: The figure shows Domain 3. The topography is visible by gray contours. The colored contours show the area where $q_v > 10$ g kg^{-1} in the lowest model layer moving over time in intervals of 30 minutes from 4 UTC to 19 UTC. Brighter contours are associated with later time steps. Visible terrain indicates that q_v never exceeded 10 g kg^{-1} at the corresponding grid point.

bution indicates orographic forcing as a likely reason. The convergence zones are mostly small and situated directly above or close to mountain peaks and ridges. At 9 UTC during August (11 am local time) one would expect a thermal circulation with northeasterly ground-relative low level winds along the southeastern slopes of mountains. The synoptic wind direction is westerly, which leads to convergence along peaks and ridges.
At 10:15 UTC the cold pool induced convergence line reaches the supercell's triggering point and increases convergence over the mountain's ridge. During this process air from the warm sector is pushed into the Alpine valleys from the north and concentrates along the mountains and directly north of them. Convergence also occurs in the region of davos, where the real storm originated. The model captures the potential for storm initiation in the original triggering zone and even produces a smaller convective storm slightly south of that area later during the simulation.

2.3.3 The Simulated Storm

After its initiation the storm moves eastward at about 14 m s^{-1} along an almost perfectly straight track. It moves north of the Wetterstein and Karwendel mountain ridges, following a weak convergence line marked **A"** in Fig. 2.12a which might be orographically induced. The low level winds advect warm air into the Inn Valley. Along the valley, the wind direction is reversed relative to the synoptic winds. Fronts can often be observed moving along the Alps from the west to the east and into the Inn valley and then up the Inn Valley from the east to the west. Other Alpine valleys can experience similar phenomena with a less drastic reverse flow. The fast moving cold air north of the Alps pushes the warm air ahead of it into the valleys, further increasing moisture and CAPE along the supercell's path. As it moves over the Inn Valley and the adjacent lower terrain

around Kufstein and Wörgl towards St. Johann in Tyrol the storm intensifies and grows significantly in size and its motion vector turn slightly south. Markowski and Dotzek (2011) speculated that an increase in intensity could alter the course of the sotrm, causing a RMS to deviate towards the right. The reason is a change in the dynamic pressure gradient along the updraft.

At this time the storm is still about 15 - 20 km north of the storm track marked by Jaeneke (2007). The intensifying updraft exceeds 30 m s^{-1} as it moves over the Kitzbühel Alps and then the Leoganger Steinberge with an almost constant updraft of over 35 m s^{-1}.

During the whole period weaker convective cells keep occurring over Switzerland. The cold pools move eastward and through the Rhine Valley. As the cold air crosses the Arlberg and encounters the warm air in the Inn Valley it triggers another convective system which shows the characteristics of a squall line. Figure 2.12b shows this system marked with **C** shortly after its formation just ahead of a strong cold pool in the Inn Valley. Its convergence zone is directly ahead of the cold pool and its updraft, visible in Fig. 2.11 is stretched in north-south direction, moving towards the east. In contrast to this, the cold pool of the supercell does not form until 150 minutes after its initialization when it becomes visible almost 30 km north of the main updraft in Fig. 2.12b, marked with **B'**. The convergence associated with the supercell core is marked with **B**. It is typical for easterly moving supercells to have their FFD north relative to their updraft core. This ensures that the cold air does not interfere with the supply of warm air from the east and southeast and helps sustain the system. The location of the cold pool also explains why there is still warm moist air left in the Inn Valley after the supercell moved very close along the valley. The squall line which is now moving behind the supercell and about 20 km south of its former track is faster than the supercell and the distance between the two systems slowly starts decreasing.

The cold pool formed by the supercell's FFD spreads and a convergence line forms along its leading edge. Eventually, a second updraft forms north of the supercell and along the gust front. This is visible in 2.12c, marked with **D'**. The system evolves from a single supercell into a squall line with a rotating mesocyclone at its southern end. The convergence zone beneath the supercell is marked with **D**. The RFD does not show clearly throughout the whole simulation. The mountainous terrain is a possible reason as it distorts the wind field. The minimum in θ_e marked with **D"** could be caused by the RFD. This configuration remains stable for about one hour before the updrafts of the supercell and multicell start moving away from each other, because the supercell moves slightly towards the south and slower towards the east. It is typical for a supercell to move slower compared to single and multicells. Right moving supercells tend to move to the right relative to the mean evironmental wind. The convergence zones beneath the supercell and the multicell to its north are visible in Fig. 2.12c, marked with **D** and within the southern part of **D'**, respectively.

The northern part of the squall line moves over the Salzkammergut where several lakes

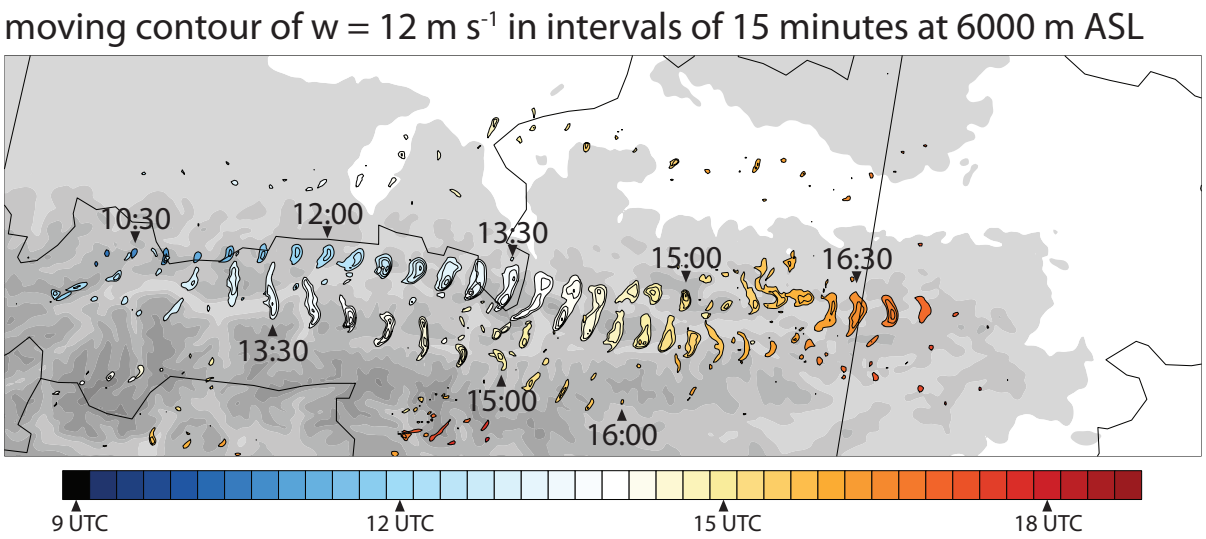

Figure 2.11: Moving contours of w at 6000 m above sea level. Each time step is drawn in its own color to illustrate the movement of different updrafts. The black solid contours are drawn in intervals of 6 m s^{-1} and reveal the most intense regions within the updrafts. The terrain is shown in grayscale with contour spacings of 500 m, white being below 500 m and the darkest gray being above 3000 m.

are situated. In addition, the topography is realtively low and just like the supercell the northern part of the squall line increases in updraft strength after moving through the valley. However, it shows a rather unsteady structure after 15:30 UTC, weakens significantly and is replaced by a second line of cells which is condiderably more distorted. It splits into two separate updrafts, the northern part dissipates after less than 30 minutes while the southern part once again forms a line. It then also weakens slowly until it becomes untrackable after 17 UTC. This is visible in Fig. 2.11.
During this time the squall line which formed in the upper Inn Valley moves south towards the Tauern and dissipates at around 16 UTC. When viewing weaker updrafts, it becomes evident that the system in the south catches up and forms a line together with the remains of the supercell and the multicell to the north which moves over the eastern Alps before the whole system dissipates. This is consistent with the surface θ_e and wind fields which show a gust front and preceding convergence line spanning the southern half of Domain 3.

2.4 Verification

To verify the simulation results, they are compared to station data and radar images. The station data is provided by the Zentralanstalt für Meteorologie und Geodynamik (ZAMG). The data from their Teilautomatisches-Wetter-Erfassungs-System (TAWES) was kindly provided by the ZAMG. The data is available in 10 minute time steps for The radar images were kindly provided by the Austro Control, which is an air navigation service

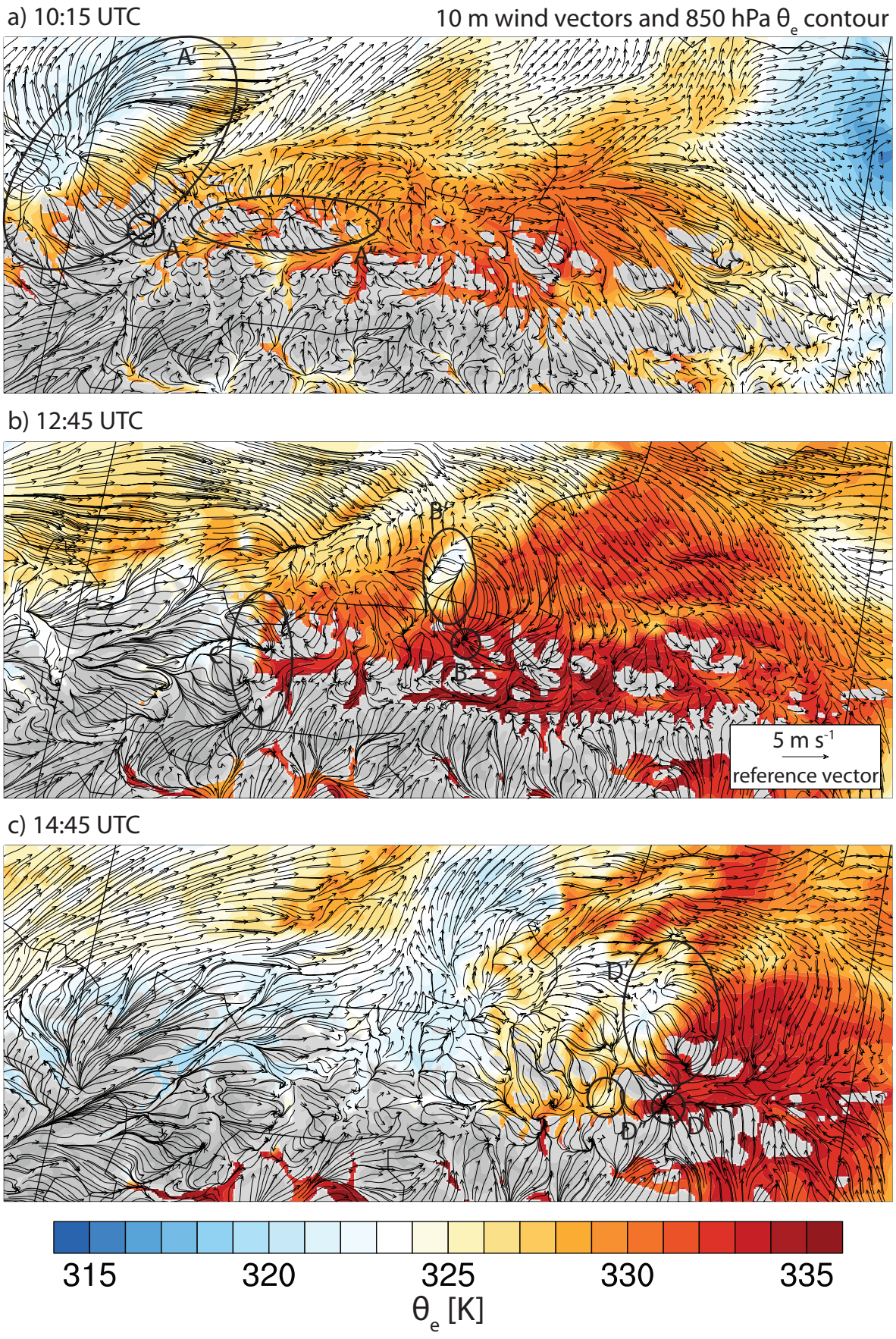

Figure 2.12: Plot of θ_e [K] at 850 hPa and 10 m wind shown as streamline following wind vectors.

provider and is in control of austrian airspace.

2.4.1 Comparison Between Model Data and Station Data

Observation data from the ZAMG's TAWES station network is used to verify the simulation results. The station data is shown along with time series of surface fields from the closest model grid point. In order to aid comparison, conversions and corrections described in Appendix B are applied to to the station data. There are several classes of stations. The first calss are most of the stations in Tyrol, which can be divided into two groups. The northern stations did not pick up the real storm but were hit by the simulated storm while the stations in the south registered the real storm while the model storm was to far north to affect them. The second class of stations is located where the most severe weather occurred. The resemblance between station and model data in this area is better than in Tyrol because the modeled and real storm tracks align well in this area. Representative examples for these two classes will be shown in detail below.
The third class of stations are those which are strongly affected by the model mechanics, such as stations within the relaxation zone or stations with large vertical displacements due to terrain smoothing. Stations which are affected the most by terrain smoothing are those located on peaks or ridges or in narrow valleys. They are displaced downward or upward on the model terrain relative to their real location. Depending on the station, the difference can be up to 600 m, although most stations are not displaced that drastically. This process not only changes the pressure and temperature but also alters the relative terrain around the grid point compared to that of the station. Consequently, for these grid points, one could expect especially the simulated wind field to be very different from the measured one.
Stations on relatively flat terrain suffer from less vertical displacement and generally show better resemblance to the measurements. However, the simulation itself exhibits important differences compared to the storm from August 2. As mentioned above, the triggering location as well as the storm track are different from reality in the simulations. Due to a slight southward tilt of the simulated storm track relative to the real track, the area which was affected by the most severe weather is also hit by the simulated storm during its most intense phase. The result is a very good resemblance between station data and simulation data in that particular area.

The Western Part of the Storm Track

This part covers most of Tyrol except for the easternmost part. While the real storm originated in Graubünden and moved east-northeast to Innsbruck in an almost straight line, the modeled storm was initiated in the Arlberg region over the boundary between Tyrol and Vorarlberg. It then moved eastward, staying north of the Inn Valley, while the real storm stayed slightly south of the Inn Valley. This results in two groups of stations,

one being located in the north of Tyrol and the other in the south. The northern stations picked up precipitation from the multicellular part of the real convective system. However, they did not register the core of the system which was located further south. The stations in the south registered the main convective cell. The precipitation for the southern stations is generally underestimated because the simulated storm was located further to the north.

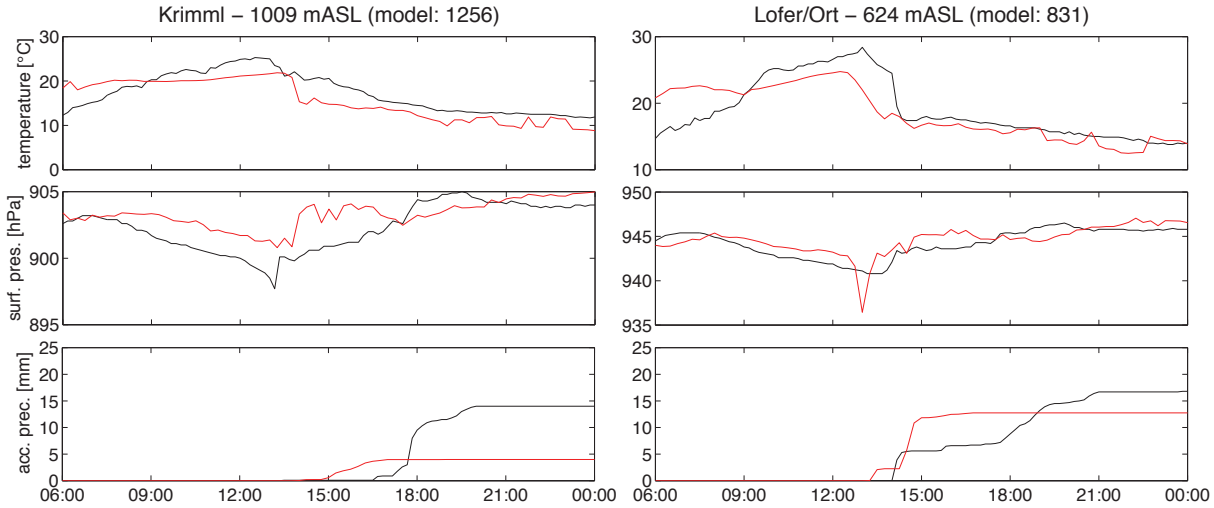

Figure 2.13: Time series of T, p_s and accumulated precipitation for stations Krimml and Lofer/Ort. Measurements are shown in black, model output is red. The x-axis shows time in hours from 2007-08-01 00 UTC to 2007-08-03 00 UTC.

Figure 2.13 shows an example for the north-south difference. Since station Krimml is located south of the simulated system in the upper Salzach Valley, it was only hit by the real storm's core and registered a strong minimum in the surface pressure when the mesocyclone passed over it. The diurnal temperature cycle is underestimated. This underestimation is common to almost all stations. The drop in temperature occurs about one hour too late and the real storm itself caused a relatively moderate drop in temperature by only 2.5 K. One other commonality to most of the other stations is the underestimated pressure drop due to the approaching cold front. The precipitation for the station was underestimated by the model by over 60%. The most obvious reason for that is the deviation of the modeled storm track from the real storm track. While the modeled precipitation accumulated within about three hours, the real event was spread over more than six hours.

Station Lofer/Ort on the other hand is located close to the border between Austria and Germany and therefore right on the track of the simulated storm's core. The result is a very sharp minimum in the surface pressure. However, even for Lofer/Ort the precipitation is underestimated and also concentrated within a shorter time period. Just like the pressure drop and the diurnal temperature cycle, this feature is present for most of the stations when the observations are compared to the model data.

The Area of Most Severe Weather

This area covers the northern part of the Salzach Valley and the upper Enns Valley. The real and simulated storm tracks intersect in this region, resulting in a very good agreement of the station data with the simulation data. However, there are some important differences, too. The deviation in the temperature and pressure cycles mentioned above is also present in Fig. 2.14. The wind direction and speed are relatively poorly modeled compared to other parameters, although there are several stations with good wind direction results, the wind speed is generally underestimated. The station representative for this class is Bischofshofen, where the modeled convective system arrives about one hour early. The relative humidity shows the same one hour lag between the the real and the simulated storm. It is directly linked to temperature since T_d does hardly change. In general, moisture is poorly represented by the model. The comparison for Bischofshofen shown in Fig. 2.14 is one of the stations with the best agreement between modeled and observed relative humidity.
The accumulated precipitation shows three separate precipitation events between 15 and 21 UTC. The model's precipitation is underestimated by a factor of 0.5 and concentrated mostly within two events, a heavy one shortly after 15 UTC and a much weaker but longer one between 16 and 18 UTC. Not all stations show equally good agreement as Bischofshofen.

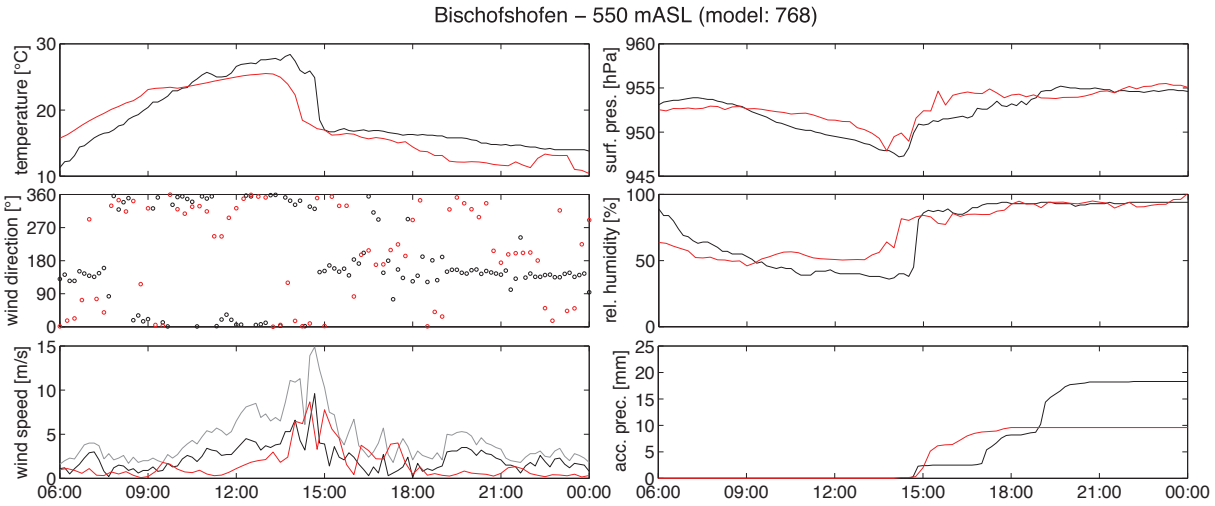

Figure 2.14: Time series for Bischofshofen, showing T, p, wind direction, relative humidity, wind speed (10 min mean in black, peaks in gray) and accumulated precipitation. Station data is black, model data is red.

2.4.2 Comparison of Simulated and Observed Radar Reflectivity

Radar images contain information about precipitation intensity and rain water contents. Especially during convective events, where precipitation is distributed very inhomoge-

neously over an area and also over time, a radar is the only instrument which can capture the instantaneous precipitation field. When using models with low grid spacings the internal structure of a mesoscale convective system is resolved and updrafts within the system are modeled. The comparison between observed and simulated reflectivity is an effective way to compare the observed and the modeled convective system. A good simulation should capture time and location of the heaviest precipitation events and the mesoscale structure of the convective system even if certain details are poorly modeled. The time steps for the radar images in Fig. 2.15 are the same as in Fig. 2.5. As mentioned above, they represent four important development states of the convective system. All of those stages were captured by the model, although not necessarily at the exact same time and place. The time steps of the model output which are compared to the observed reflectivity are chosen to show stages of similar development rather than the same time.
The simulated storm is initiated at a different time and location compared to the real storm, which causes subsequent time steps to differ from the real storm. The simulated initiation took place about 45 minutes prior to the real initiation and slightly further east, resulting in a model storm running about 1 hour ahead of the real storm. The first time step with a visible signal of the storm for both real and simulated storms are shown in Fig. 2.15a at 10:00 UTC and 9:45 UTC respectively.

The steps shown in Fig. 2.15b-d account for the lag by showing the model time step one hour earlier than real time, resulting in better comparison of the supercell's position in both images. Resulting from the chosen reference latitude the map for the model output is tilted slightly clockwise. While the real storm already shows multicellular development along a line oriented toward north, the modeled storm still shows the structure of a single supercell in Fig. 2.15b. The development of a powerfull secondary updraft directly north of the storm is visible in the radar image of Fig. 2.15c. No clear secondary maximum is visible in the model reflectivity. However, a clear secondary updraft at 13:45 UTC model time is visible in Fig. 2.11. A squall line is forming over the upper Inn Valley, visible on the radar image. At the same location the simulation shows a convective line, but its initiation takes place about 2 hours earlier in the model. The distance between the two systems in the model output is only about half of the observed distance. Since the images are taken at two different times, the real discrepancy between the two squall lines is even greater.
Figure 2.15 shows the final stage of the system. The supercell is still visible at the right side of the radar image, clearly standing out from the convective system towards the southeast. The model storm looks significantly different at this time with the supercell well embedded into several secondary updrafts. This also shows the above-mentioned development into a single curved line during the simulated system's decay. The large system directly west of the real super-multicell results from the above-mentioned squall line and in the model run it dissipates to to its proximity to the main storm.

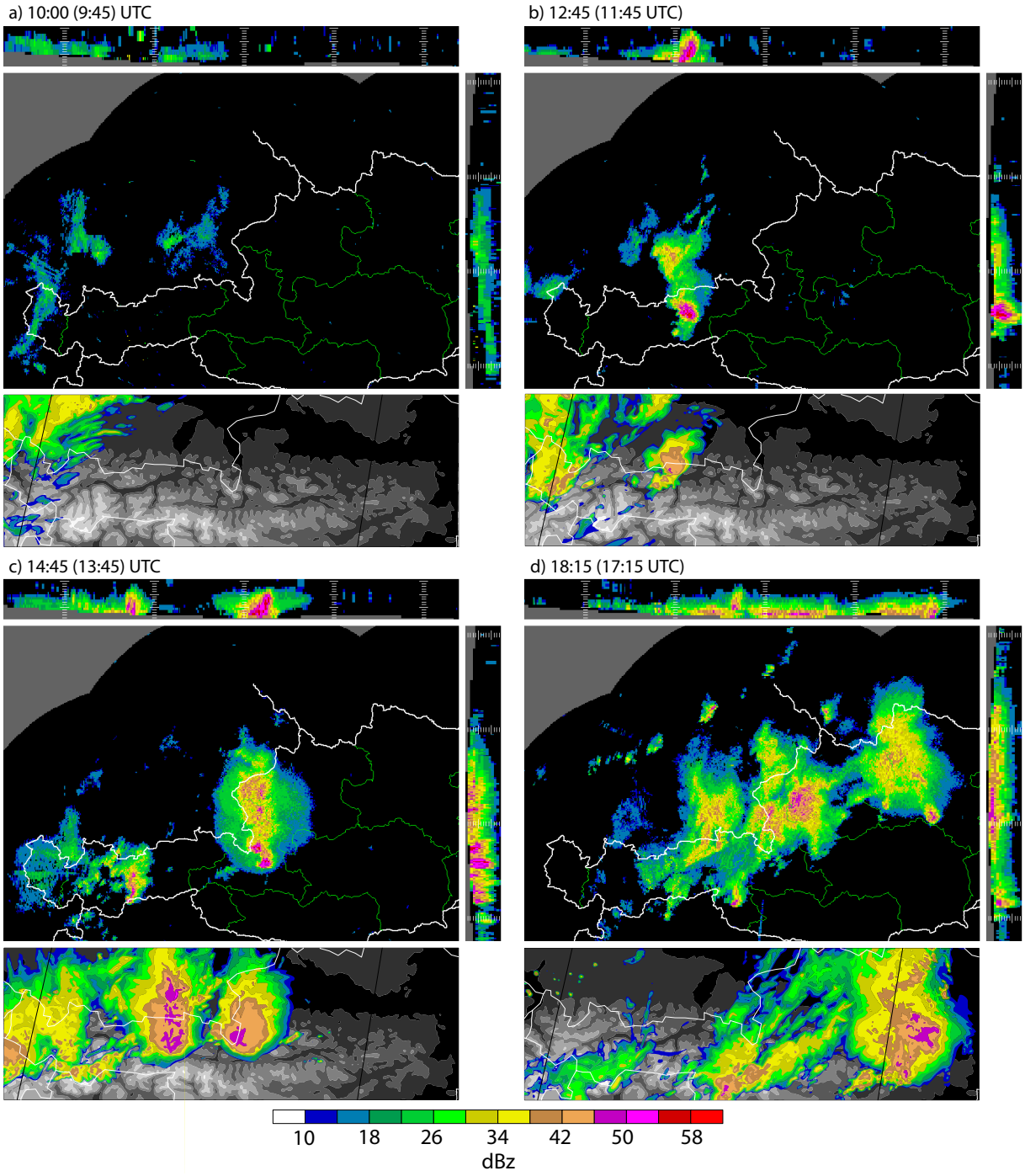

Figure 2.15: Comparison between radar images (top) and simulated reflectivity (bottom). Observations as in 2.5. For each subplot, the real time (model time) is given. The simulated reflectivity is the maximum for each vertical column. The area shown is the corresponding part of Domain 3. (radar images © Austro Control)

Despite the differences, Fig. 2.15 shows that there are several important features of the storm which were captured by the model. The squall line which formed after the supercell is simulated relatively well until it starts interacting with the main storm. A smaller convective storm forming over Osttyrol, visible in Fig. 2.15d in the lower center, is captured by the model; however, it occurs about 1 hour early. The total maximum

reflectivity in the model is lower than the measurements. This might also be a result of the resolution, as simulated storms are able to form narrower and more powerful updraft cores as the horizontal resolution is increased.

2.5 Interaction of the Modeled Storm with the Terrain

In order to understand the effect of the terrain on the storm it is important to examine the development over time and connect it to imortant parameters which influence the updraft intensity. Following Markowski and Dotzek (2011), who identified the change of CIN and CAPE due to terrain obstacles as the most important influences on storm evolution, Fig. 2.16a shows the maximum updraft intensity within the supercell core for each time step along with a two-dimensional cross section through the terrain along the storm's path in Fig. 2.16b, CAPE in 2.16c and CIN in 2.16d. The resolution of the terrain plot in panel b is 10 times higher than that of the graphs shown in panels a, c and d in order to account for narrow ridges and valleys which the storm encounters between the model output time steps. Plotting the terrain only at the locations of the supercell at the output time steps, between which the storm travels about 15 km, would eliminate important terrain features such as the Salzach Valley which have a visible effect on storm intensity. The solid, long dashed and short dashed lines show the values 15, 30 and 45 minutes prior to the storm's arrival at a given grid point and are a horizontal average over the maximum values in each vertical column 4.2 km around the storm's core, which is given by the maximum value of vertical velocity within the core for each given time step. The averaging ensures that locally confined strong maxima or minima of CAPE don't distort the data.

A first examination of Fig. 2.16 shows a time shifted correlation between low (high) terrain and an increase (decrease) in updraft intensity. One of the interesting findings is that - according to the model - a severe storm occurred even though the CAPE values along the track were moderate at best, never exceeding 1200 J kg^{-1}. The CAPE used in this figure is the maximum within a vertical column. The maximum is not necessarily at the surface since the convective circulation can move moist air over drier air, resulting in higher CAPE aloft. Another important fact are the very low CIN values along most of the storm's track.
During its first two hours the storm encountered three obstacles (Lechtal Alps, Wetterstein and Karwendel) separated by relatively narrow valleys. The time series in Fig. 2.16a shows an increase in intensity by more than 5 m s^{-1} after both valleys and a stagnation or even a drop after all of the three mountain ranges. The CAPE is still relatively low in the area the storm crosses during its first hour of development and almost constant over time while the CIN is relatively high but decreases by more than 60% within 30 minutes prior to the storm's arrival. Convergence present in the area could be a possible reason

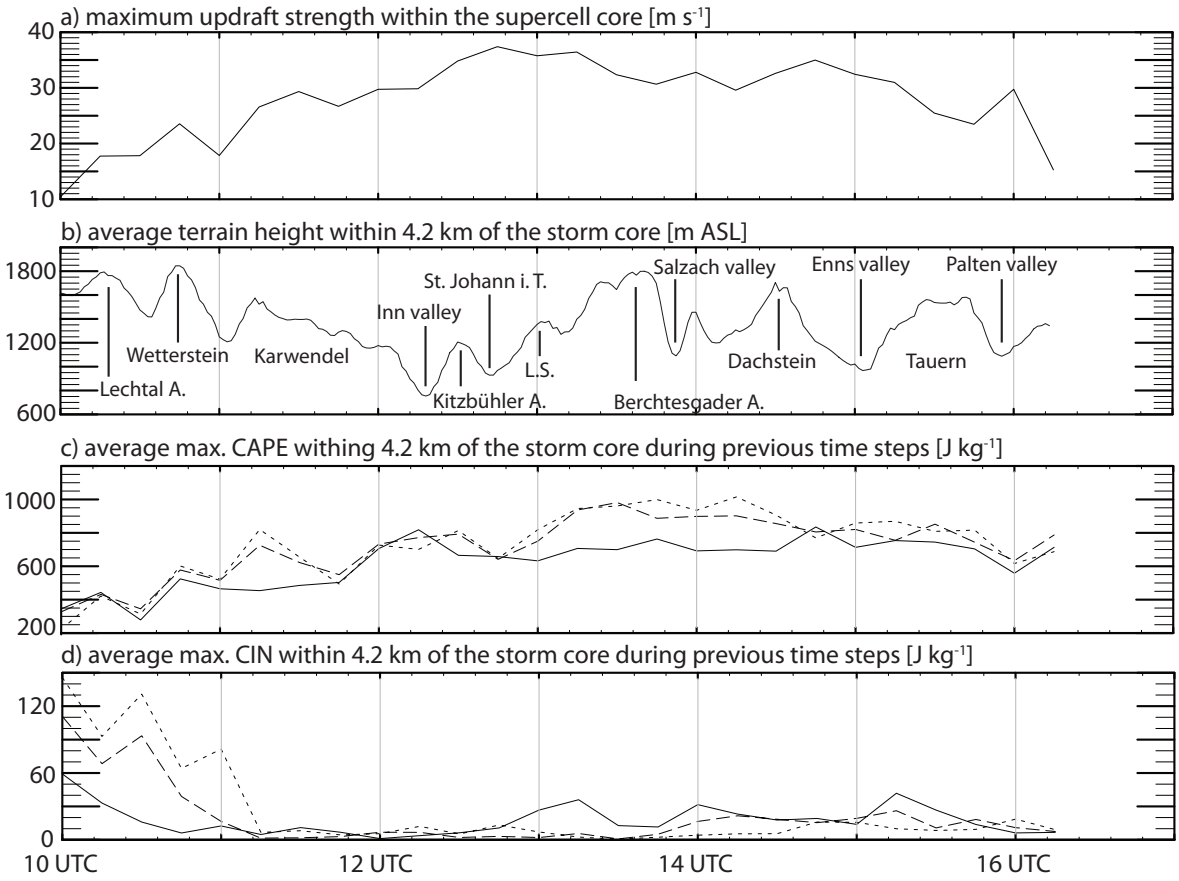

Figure 2.16: (a) maximum supercell updraft strength over time, (b) average terrain height within 4 km of the max. updraft, L.S. is short for Leoganger Steinberge, (c) and (d) average max. CAPE and CIN within 4 km of the current storm core as in the model output of the previous three time steps with the solid, long dashed and short dashed line indicate 15, 30 and 45 minutes prior to the storm core's presence. CAPE and CIN fields contain the maximum for each vertical column and are then horizontally averaged.

for the decrease in CIN due to the lifting of air. The storm's intensity also correlates well with the CAPE values at the given locations. Without analyzing further development the influence of CAPE and terrain cannot be separated.

Between 12 and 13 UTC the storm moves through the lowest point of its track in the Inn Valley and gains further strength afterwards. The updraft intensity also increases slightly while the storm moves down from the Karwendel into the Inn Valley - this is accompanied by a significant rise in CAPE from 500 to 800 J kg^{-1}. However, even in an environment of slightly decreasing CAPE the storm strengthens even faster than in higher CAPE environments while it leaves the Inn Valley and moves over St. Johann in Tyrol. The following slight decrease in intensity is accompanied by zone of higher CIN through which the storm moves between 13 and 13:30 UTC. However, the strongest decrease in intensity is observed while the storm is directly over Berchtesgader Alps where CAPE is higher and CIN is lower than during preceeding time steps. Along with the good agreement of updraft intensity changes with the terrain height, this is a very strong indication that the terrain might be responsible for intensity variations by inducing thermal circulations.

Below it will be shown that the thickness of the CAPE layer is highly variable along the storm track.

For example, at 14 UTC the updraft has gained strength while CAPE has dropped and CIN has risen, but shortly before 14 UTC the storm moved over the Salzach Valley, which is almost 1000 m lower than Berchtesgader Alps. During the following hour, the same pattern can be observed two more times while CAPE and CIN do not match the observed changes in intensity. Finally, after 15 UTC the storm begins to weaken significantly even after passing through the Enns Valley and after one last intensity peak at 16 UTC shortly after moving through the Palten Valley, becomes hardly trackable as a supercell with intensities well below 15 m s^{-1}.

From comparing the CAPE values in Fig. 2.16c 15, 30 and 45 minutes before the storm's arrival it appears the values seem to decrease as the updraft approaches. However, this is an effect of the way the CAPE is calculated in equation 1.13. Buoyancy for an upward moving parcel is integrated from the LFC up to the EL. The values of θ_e in the middle troposphere are around 325 K in the prestorm environment and increase up to 331 K in the center of the updraft. The same applies for T. As the storm approaches, the middle troposphere gradually warms and the result is a lower buoyancy when moving a parcel vertically up through the troposphere. The calculation of CAPE directly within the updraft does not yield meaningful results at all since in the rising column of air $d\theta_e/dz \approx 0$ and therefore CAPE ≈ 0 even within a very strong updraft.

The interpretation of the time series in Fig. 2.16 yields an interesting connection between

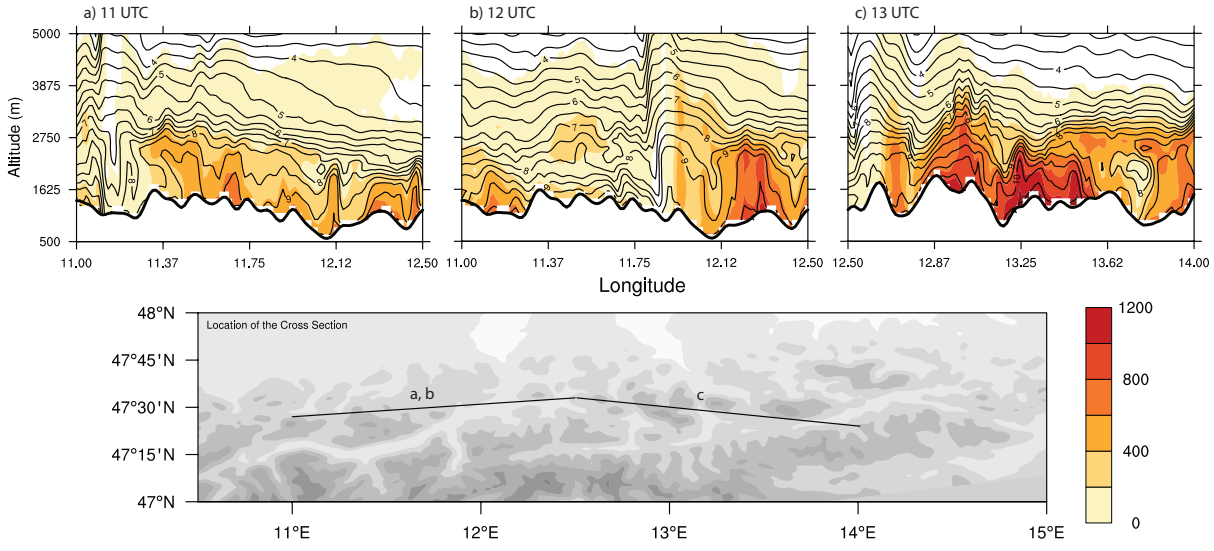

Figure 2.17: Along-track vertical cross sections showing CAPE [J kg^{-1}] in color and q_v [g kg^{-1}]. The map shows the locations of the cross sections.

updraft strength and terrain height. To clarify the mechanism behind this connection Figure 2.17 shows cross section through the prestorm environment along its track. Fig. 2.17a and b are taken along the track where it crosses the Inn Valley. The cross sections reveal that the center of the valley shows a lower concentration of water vapor and a much

more shallow CAPE layer than over the Karwendel west of the valley and the Kitzbühl Alps to the east. They also show how the depth of the CAPE layer increases from 11 UTC to 12 UTC.

Ahead of the storm the CAPE and q_v fields align very well. However, as the storm approaches, CAPE gradually decreases directly ahead of it. The reason for this decline is explained above. The storm is located within all three of the cross sections. It is situated at 11.1, 11.8 and 12.6 degrees east in Figs. 2.17a, b and c respectively. The alignment of CAPE and q_v is easily explained by the presence of higher amounts of latent heat. The Inn Valley and the Salzach Valley are both characterized by a minimum in moist layer depth ($q_v > 9$ g kg^{-1}) above their center. Figure 2.17 reveals a possible reason for the weakening of the storm even though CAPE in 2.16c shows no decline, which could explain the weakening of the updraft. A pocket of drier air is located over the Enns Valley, located at the eastern end of Fig. 2.17c. These variations in CAPE layer depth do not necessarily show up in plots showing the maximum CAPE for each vertical column. However, they cause large variations in the total energy which is available to the thunderstorm. The concentration along slopes close to valleys could be caused by thermal circulations which lead to convergence over the adjacent taller terrain features.

Chapter 3

Sensitivity Tests

3.1 Changes in the Model Topography

In order to test the influence of the topography on the storm event described in Chapter 2, the model terrain has been modified to reduce the small and large scale terrain features in two steps. The purpose of these experiments is to show that the conditions as encountered on 2007-08-02 are dependent on the presence of the Alps as a whole as well as the more complex features of the northwestern Alpine region. In the first step the fine structure of valleys, ridges and peaks was removed from the Alps, resulting in a single smooth ridge representing the whole mountain range. This was achieved by interpolating the terrain from Domain 1 onto the finer grids of Domains 2 and 3 and then interpolating the meteorological fields over the smooth topography. Initial attempts with smooth topography showed that the smoothing reduced the overall height of the terrain drastically, resulting in relatively short central Alps. To compensate this effect, a stretching function f_1 was introduced.

$$f_1(x,y) = \frac{G-H}{H(H-C)^2} * (h(x,y)-C)^2 + 1, \tag{3.1}$$

Where $h(x,y)$ is the regular terrain at the grid point (x,y), $H = \max(h)$, $G = 3500$ m is the desired maximum height of the modified terrain and $C = 1000$ m is the threshold above which the terrain should be stretched. The stretched terrain $h_s(x,y)$ is given by

$$h_s(x,y) = \begin{cases} h(x,y) & \text{for } h < C \\ f_1(x,y) \cdot h(x,y) & \text{for } h \geq C. \end{cases} \tag{3.2}$$

This grants a smooth transition between stretched and non-stretched terrain and stretches only a relatively small area up to G m above sea level. The terrain below C is not altered, higher terrain is stretched by a factor between 1 and G/H. The modified terrain $h_s(x,y)$ was used as new terrain height field in Domain 2. Initial tests revealed that the original position of Domain 3 was too far north to capture the convective system under these new conditions properly, which is why it was moved south by 50 km relative to its position in

the control simulation.

To test to which extent the Alps were responsible for the conditions which led to the storm, another test was conducted. The second step was to remove the whole Alpine ridge. In order to keep the prestorm conditions around the Alpine region as close to the control run as possible, the only terrain feature removed from all domains is the Alpine ridge. This was achieved by first running the WRF preprocessing system for all three domains to generate the geographical fields. The following algorithm was used to remove the Alps from Domain 2. The flattening process requires a weighting function

$$f_2 = \max\left[\frac{1}{2}\left(1+\cos\left(\frac{2\pi x}{N_x}\right)\right)^{26}, \frac{1}{2}\left(1+\cos\left(\frac{2\pi y}{N_y}\right)\right)^{26}\right], \tag{3.3}$$

where x and y are the grid point coordinates within Domain 2 and N_x and N_y are the number of grid points of Domain 2 in x and y direction respectively. The values of g range from 1 along the boundary of the domain to 0 in the center. This was used to replace the terrain within Domain 2 without modifying the boundaries and grant a smooth transition between replaced and original terrain. The flat terrain h_f was obtained from the original terrain h by

$$h_f = \begin{cases} h & \text{for } h < 400 \\ f_2 \cdot h + (1 - f_2) \cdot 400 & \text{for } h \geq 400. \end{cases} \tag{3.4}$$

This algorithm replaces terrain higher than 400 m with a flat plane with an altitude of 400 m except for the boundaries of the domain, where a continuous transition between flat and original terrain is achieved. The results with altered topography are described below.

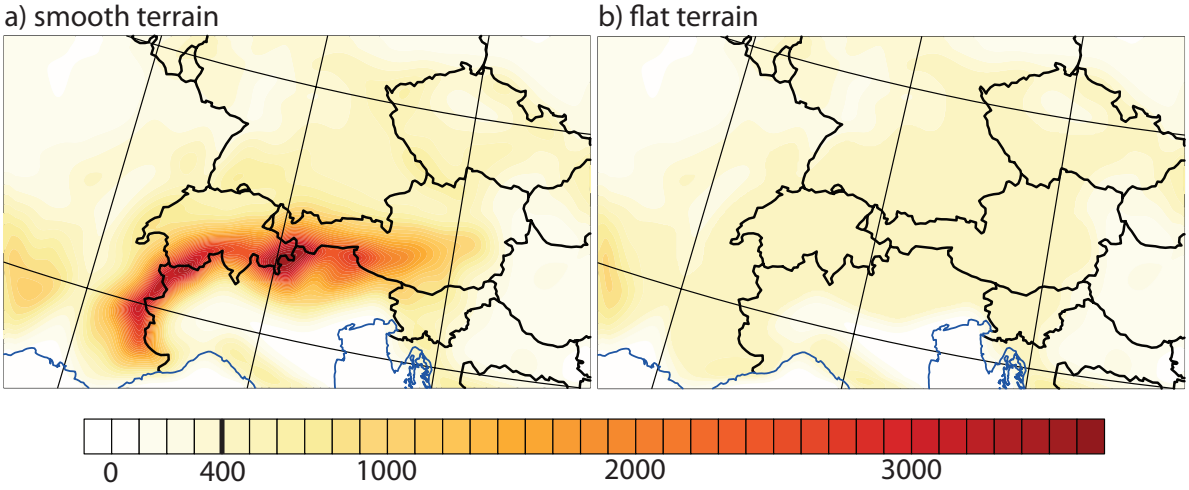

Figure 3.1: Contour plot of the model terrain of domain 2. The thick black line in the label bar marks the height of the plateau seen in (b).

3.2 Results with Altered Topography

For simplicity, the simulation documented in Chapter 2 will be referred to as control simulation in this chapter. Likewise the terms control storm and control supercell will be used to refer to the corresponding features of the simulation above.
The smooth terrain simulation shows a drastic change in storm evolution and behaviour. Instead of a long lived supercell-multicell system, several components with a less continuous life cycle develop. Figure 3.2 shows the updraft movement over time for the smooth terrain simulation. The earliest system visible in the figure is initiated at around 10 UTC almost at the same location as the main system in the control simulation, yet it dissipates in less than 90 minutes and never reaches the intensity of its control simulation counterpart. The development along almost the path of the control storm continues later and a relatively weak system moves over the border region of Germany and Salzburg towards east-northeast. There are more cells evolving in the area, but while their paths are almost parallel, they evolve at different times.

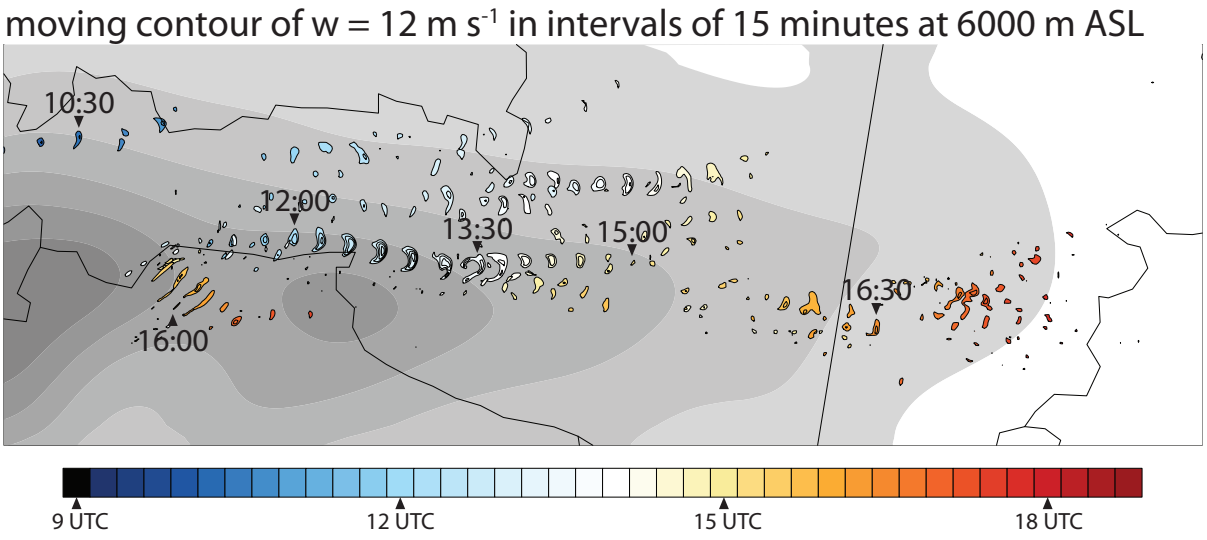

Figure 3.2: Same as fig. 1 but for the smooth terrain simulation.

Farther to the south, just north of the border between Austria and Italy and along the steepest terrain, a supercell forms at around 12 UTC and moves eastward. The shape of the updraft is very close to those of the simulations done by Weisman and Klemp (1982), which is not surprising since the cell can evolve much more like its ideal counterpart over the smooth terrain than in the control simulation. However, it is relatively short-lived compared to the supercell in the control simulation. At 13:30 UTC the shape has already drastically changed and the supercell character of the storm is lost shortly thereafter.

In the flat terrain simulations the effect of the Alps becomes apparent. Their role in this particular case is to provide the change in the wind field which is necessary to generate

supercells in the first place. The system moves over the flat plateau relatively undisturbed and neither the cold front nor the warm front are disturbed by any larger obstacle. The transport of latent heat into the lower troposphere via boundary layer processes is evident through an examination of the 10 m wind and θ_e fields that show an increase of θ_e over time that cannot be explained by advection. The importance of this process is enhanced in this highly idealized scenario, because the low level winds are not influenced by any orographic obstacles.

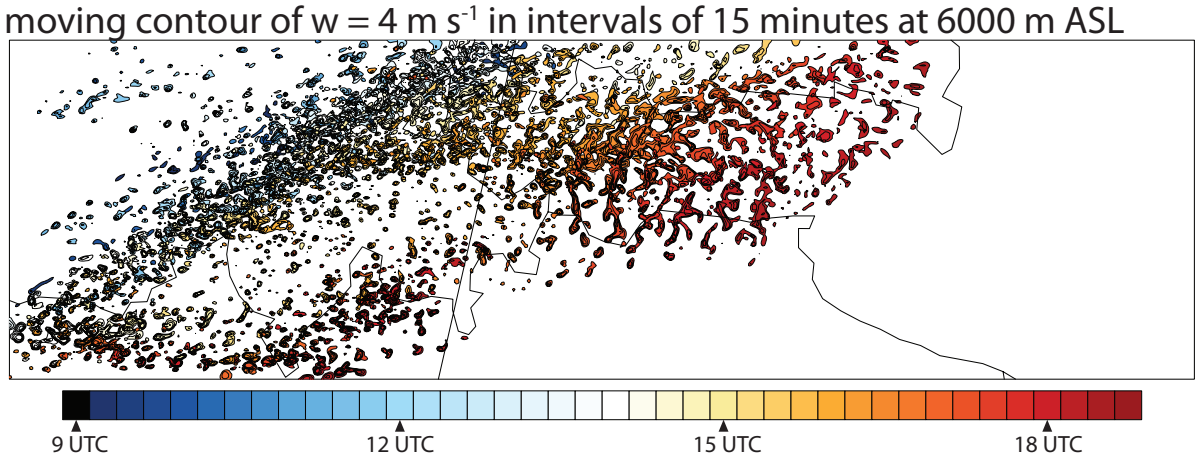

Figure 3.3: Moving contours of w at 6000 m above sea level. Each time step is drawn in its own color to illustrate the movement of different updrafts. The black solid contours are drawn in intervals of 4 m s^{-1} and reveal the most intense regions within the updrafts.

The cold front passes over the plateau which is placed in Domain 2 instead of the alps. Without the Alps blocking the airflow, the warm air moves ahead of the cold front towards the east and is not lifted. The surface wind field shows none of the convergence zones which form in the control simulation. The surface properties are not altered in this simulation, only the height of the terrain. This indicates that the convergence in the control simulation is in fact related to the topography, which is a necessary condition for the formation of thermal valley circulations.

Without the supporting convergence and orographic lifting convection develops much later and in a very different way than in the control and even the smooth terrain simulations. Instead of forming a long-lived supercell the cold front triggers a series of thunderstorms which organize into a squall line which then moves ahead of the cold front towards the east. Figure 3.4 shows the cold pools which form between the cold front and the gust front. The surface cold front is located in the northwest over central Switzerland in 3.4 while the gust front is ahead of the cold front, indicated by the convergence line, which ranges from northern Italy through Tyrol into Germany.

The movement of updrafts over time is shown in 3.3. The most striking difference to the control and smooth terrain simulations is the apparent absence of long lived east moving

cells. Instead, convection occurs in an almost straight line spanning Domain 3 from the north to the south along a line ahead of the cold front. This is a typical development for cells which are initiated along a line in a highly unstable environment. The scale of the colored contours is different for, namely 4, 8, 12 and 16 m s^{-1} for Fig. 3.3 as opposed to 12, 18, 24 and 30 m s^{-1} in the corresponding figures for the control and smooth terrain simulations. This is necessary to visualize the weaker updrafts.

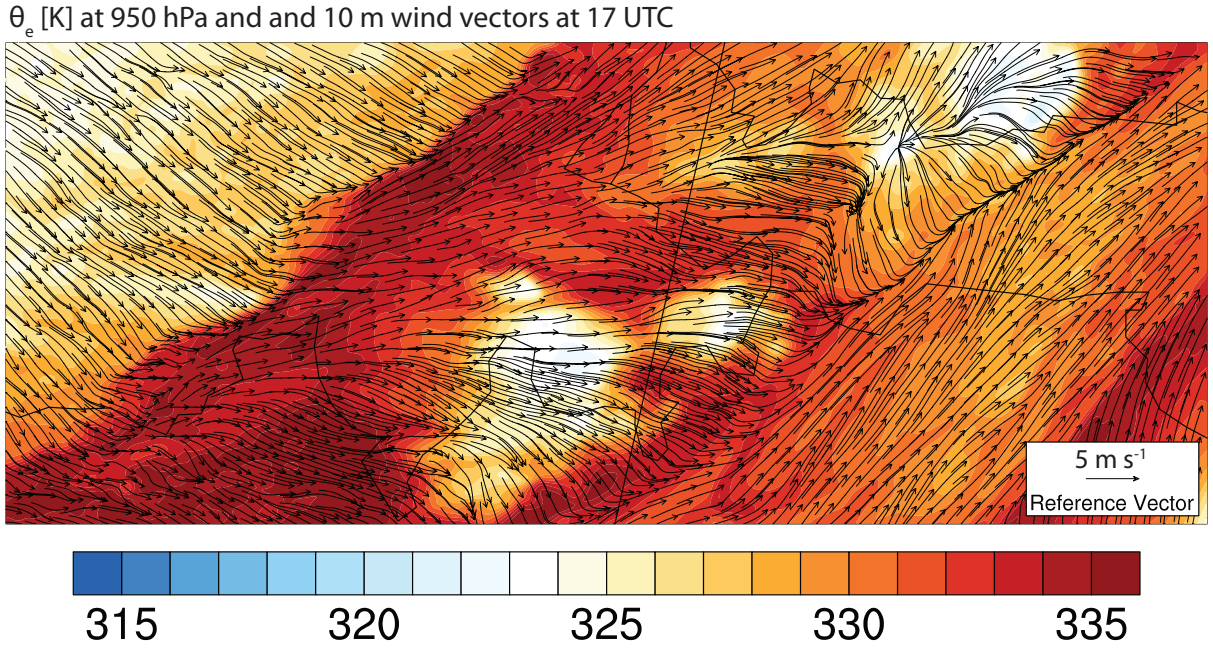

Figure 3.4: 950 hPa θ_e and 10 m streamline following wind vectors over flat terrain.

In order to understand the different development of the convective systems in the three simulations, the hodographs are shown in Fig. 3.5. The vertical change of the environmental wind with height is one of the most important factors that determine the shape of a convective system. In fact, complex convective systems only form in the presence of strong vertical wind shear. The four hodographs shown in Fig. 3.5 are all extracted from the corresponding model runs. Their timing and location was chosen 30 minutes before the storm's arrival at the location of its highest intensity.

Hodographs from Fig. 3.5a and b are taken from the control simulation. Hodograph a was extracted over the salzach valley 30 minutes before the storm's arrival. It shows clear counterclockwise turning shear with a magnitude of almost 30 m s^{-1} between 0 and 6 km. The strongest shear is encountered between 0 and 3 km, which increases the presence of shearing vorticity in these layers. In contrast, the hodograph shown in Fig. 3.5b is taken over the Inn Valley 30 minutes before the arrival of the squall line at the location of its highest intensity. While the magnitude of shear between 0 and 6 km is almost equal compared to hodograph a, its shape differs significantly. The southerly wind component between 0 and 3 km is much weaker and the shape of the hodograph is much closer to a straight line.

The hodograph shown in Fig. 3.5c is taken from the smooth terrain simulation 30 minutes prior to the arrival of the supercell at the location of the its highest intensity. Its shape up to 6 km is very similar to that of hodograph a. Figure 3.5d shows the hodograph from the flat terrain simulation, taken 30 minutes ahead of the squall line at the location of its highest intensity. Just like hodograph b it shows less curvature. The magnitude of shear is also much less with only about 15 m s^{-1} within the lowest 6 km. The wind speeds are generally lower within that layer. Just as one would expect, the storm develops into a squall line which moves slower than the systems in the control and flat terrain simulations. The absence of high vertical wind shear favors the triggering of new cells ahead of the updraft instead of the continuous motion of long lived updrafts. This is evident in Fig. 3.3, especially during the early stages of the system. The mid and upper level winds increase in strength during the day with the trough towards Domain 3. This development is apparent in Fig. 3.3 by the formation of stronger, larger and faster moving cells over Tyrol later during the day compared to small and slow moving unorganized convective cells during the moring and early afternoon over Switzerland.

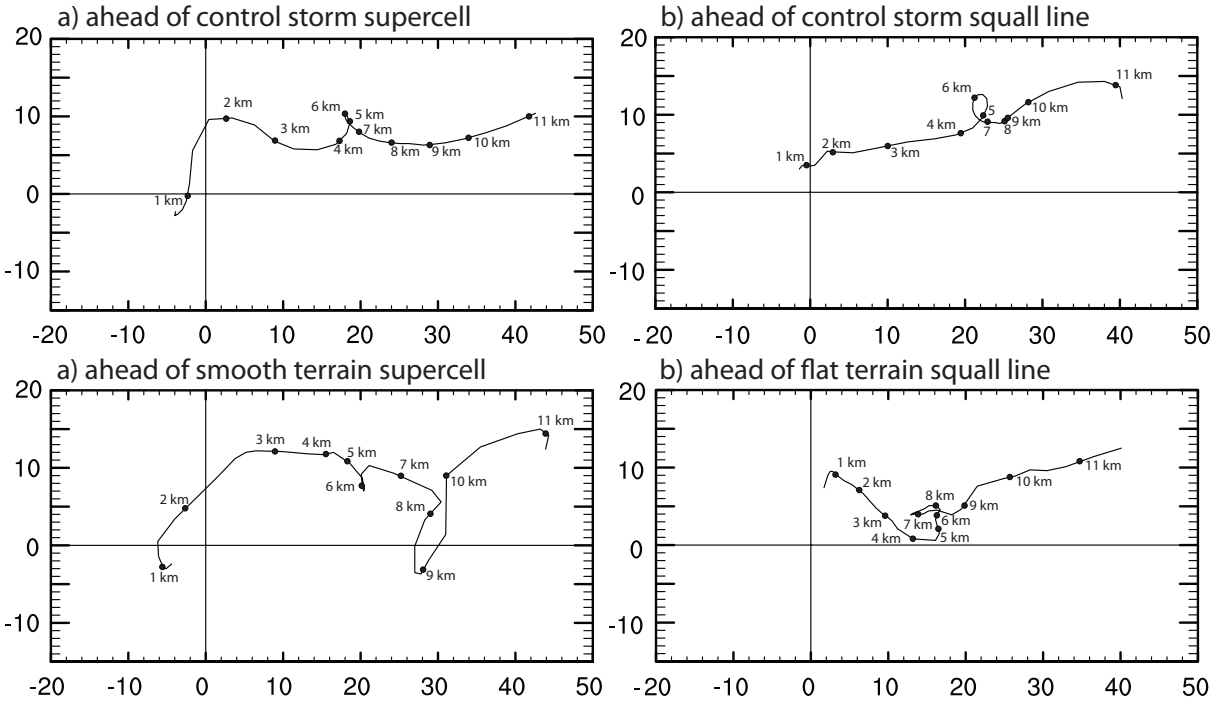

Figure 3.5: Four hodographs exctracted from the simulations. a and b were extracted ahead of the supercell and the squall line respectively. c shows the wind field ahead of the supercell in the smooth terrain simulation and d shows the wind field ahead of the

Chapter 4

Conclusions and Discussion

4.1 Summary

A severe storm event in the Alpine region was selected to investigate the effect of complex terrain on convective cells. The case was selected based on the severity of the convective system and its interesting structure. The sensitivity simulations were designed and executed to examine the effect of small and large scale features of the Alpine terrain.
The results show that even though convection and, especially, convective initiation is difficult to capture for weather models, the system evolved in a similar manner as it did in reality. The real-data simulation can be considered successful. Several ways of vertification were used to determine the similarities and differences between the simulated storm and the real storm, including radar images, station data, satellite images and soundings. The event is characterized by several factors which worked together to provide ideal conditions for the formation of a supercell storm over high mountains.

Prestorm Conditions and Large Scale Orographic Effect

- The low pressure system with its cold front provided the initial lifting which triggered convective cells over France and Switzerland. The cold air from the downdrafts of those thunderstorms was advected towards the Alps and triggered new cells.

- The Alps provided an orographic barrier which blocked the warm air on its way south. It was pushed into the valleys along the northern flanks and forced to rise. The airflow around the Alps provided vertical wind shear which was necessary for supercellular development. Sensitivity tests without the Alps have shown that the storms would have evolved into a squall line without rotating cells.

- The conditions which supported both supercells and multicells led to the growth of several severe secondary convective systems along the convergence lines ahead of the old and active cold pools as they were advected into the regions with warmer air.

Case Details and Simulation Results

The comparison with measurements, radar data and satellite images shows that several important features were captured by the model simulation. Simulations over complex terrain still pose a great challenge to modelers and models alike. During the process of this work difficulties were encountered when working without slight smoothing of the terrain. Numerical instabilities are a problem when simulating over complex terrain. Orographic lifting can cause vertical motions large enough to make the model unstable.
The simulations were carried out with a horizontal grid spacing of 833.33 m with an inner Domain 3 with a size of $750x167$ km. Higher resolutions and larger domains would have been desirable. Domain boundaries introduce unphysical disturbances due to the smoothing which is applied along them. The resolution and dimensions of the innermost domain is a resonable compromise when considering the large area which was affected by the real storm, which travelled over 420 km in the west to east direction and extended over more than 100 km from the north to the south.

- The fine structure of the Alps affected the exact position and intensity of the convective system. Diurnal heating along the slopes of the mountains and the resulting thermal circulation within valleys caused convergence. This process initiated thunderstorms and also supported their development after initiation.
- The model captured the potential for long-lived supercell storms and simulated a mesocyclone which can be tracked for over 6 hours.
- The development of secondary cells along a line north of the supercell was reproduced. However, the line was not as long as it was in reality and it was initiated later.
- A squall line which formed behind the primary system was simulated and its initiation happened too early. The reason could be the overestimated convection over Switzerland prior to the initiation of the supercell which produced a large cold pool. The cold air was advected over the Arlberg and triggered the squall line.
- The zone of highest intensity was very similar in the model and in reality. Even in the area where the simulated storm track was north of the real track the intensification of the supercell was simulated.
- The simulated reflectivity is smoother than the measured reflectivity. The limited horizontal resolution is a possible explanation. The intense peak reflectivities of over 58 dBz (Austro Control) and 64 dBz (DWD) as shown in the radar images were not simulated. The modeled storm's strongest simulated radar reflectivity was slightly below 54 dBz. Finer grid spacing might have supported higher updraft velocities in narrower updrafts and therefore higher reflectivities.

The Interaction of the Storm with Terrain

The storm's interaction with the terrain is very complex. The case study indicates that fully idealized simulations might not be sufficient to understand how convective systems and, especially, supercells are infuenced by orographic obstacles. In this particular case the system showed almost no change in direction during its existence. However, earlier studies have shown that the movement speed and direction depend only on the environmental wind.
The work by Markowski and Dotzek (2011) attempted to better understand the effect of mountain ridges on supercells. The results of this case study indicate that their results also apply to storms over much more complex terrain. Even during its steady-state phase the mature storm is supported by thermal boundary layer circulation which is a result of the diurnal cycle within valleys.
The sensitivity tests included removing the fine scale and the large scale structure of the Alps. While they provided valuable insight into the mechanisms that shaped the storm on August 2, more tests would have been disirable. Especially an ensemble like it was used by Hanley et al. (2011) would have made it much more likely to produce a system more similar to the real storm. The ensemble approach is well suited for the stochastic nature of the convective boundary layer and in consequence for the correct triggering location and time of the convective system. The tests have shown the important role of the orographic obstacles in this case.

- It remains unknown whether a movement at a different angle relative to the main ridge would have yielded such a steady system or if the corresponding wind profile could possibly occur so close to tall mountain ridges.

- Vertical cross sections through the prestorm environment show that while the maximum CAPE does only show small variations, the depth of the CAPE layer varies. The intensification of the storm shows to be related to areas with deeper CAPE layers, because more energy is available to the storm. The two-dimensional x-y-field of maximum CAPE does not contain enough information to explain the intensity changes of the supercell. Deeper layers of high CAPE contain more total energy and thus the vertical distribution of CAPE is important.

- The real storm followed wide and deep valleys along the Alps. This seems to be forced by the environmental winds rather than the presence of warmer and moister air within the valleys. In fact, the distribution of CAPE in the vertical cross sections shows that the warm moist air is not encountered at the base of the valleys.

- Since the thermal circulation is a result of radiation and surface fluxes, simulations done without boundary layer physics would neglect very important processes. The boundary layer on warm summer days is characterized by convective mixing. The

termal circulation at the scale of the valley diameters was captured by the model. However, smaller scale processes are involved in the boundary layer convection.

- The poor prediction of moisture variables such as T_d, RH and q_v compared to the station data could be a result of these convective mixing processes. Even though the stations and surface model data are located well below the layer with the most inhomogeneous CAPE and moisture distribution, the lack of a very high vertical resolution above the ground could allow disturbances to change the surface fields. However, this remains subject to speculation and only further research can clarify it.

The model study revealed several mechanisms which influence convective storms over complex terrain. However, even the control simulation was done with slightly smoothed terrain. Simulating over very high resolution terrain with $\mathcal{O}(100\ m)$ without smoothed terrain would pose a logical next step in exploring thunderstorms over mountains. With the rapidly growing computational power which is available to researchers around the world it is only a question of time until such studies are possible even for events like the one discussed in this work.

Bibliography

Adlerman, E. J. and K. K. Droegemeier, 2002: The sensitivity of numerically simulated cyclic mesocyclogenesis to variations in model physical and computational parameters. *Mon. Wea. Rev.*, **130**, 2671–2691.

American Meteorological Society, 2012: Standard atmosphere - AMS glossary. http://glossary.ametsoc.org/wiki/Standard_atmosphere.

Bryan, G. H., J. C. Wyngaard, and J. M. Fritsch, 2003: Resolution requirements for the simulation of deep moist convection. *Mon. Wea. Rev.*, **131**, 2394–2416.

Bunkers, M. J., 2002: Vertical wind shear associated with left-moving supercells. *Wea. Forecasting*, **17**, 845–855.

Frame, J. and P. Markowski, 2006: The interaction of simulated squall lines with idealized mountain ridges. *Mon. Wea. Rev.*, **134**, 1919–1941.

Hanley, K. E., D. J. Kirshbaum, S. E. Belcher, N. M. Roberts, and G. Leoncini, 2011: Ensemble predictability of an isolated mountain thunderstorm in a high-resolution model. *Quart. J. R. Met. Soc.*, **137**, 2124–2137.

Hantel, M., 2006: *Skriptum theoretische Meteorologie*. Facultas, Wien.

Holton, J. R., 2004: *An introduction to dynamic meteorology*. Elsevier Academic Press, Burlington, MA.

Jaeneke, M., 2007: Eine super-multizelle überquert die alpen. http://www.unwetterstatistik.at/analysen/schwergewitter/2007/3.pdf.

Klemp, J. B. and R. B. Wilhelmson, 1978: The simulation of three-dimensional convective storm dynamics. *J. Atmos. Sci.*, **35**, 1070–1096.

Markowski, P. and Y. Richardson, 2006: On the classification of vertical wind shear as directional shear versus speed shear. *Wea. Forecasting*, **21**, 242–247.

Markowski, P. and Y. Richardson, 2010: *Mesoscale meteorology in midlatitudes*. Advancing weather and climate science, Wiley-Blackwell, Chichester, West Sussex, UK ; Hoboken, NJ.

Markowski, P. M. and N. Dotzek, 2011: A numerical study of the effects of orography on supercells. *Atmos. Res.*, **100**, 457–478.

Murray, F. W., 1967: On the computation of saturation vapor pressure. *J. Appl. Meteor.*, **6**, 203–204.

Ortner, C., 2008: Analyse der konvektiv verfügbaren potentiellen energie (CAPE) im alpenraum. Diploma thesis, University of Vienna.

Reeves, H. D. and Y.-L. Lin, 2007: The effects of a mountain on the propagation of a preexisting convective system for blocked and unblocked flow regimes. *J. Atmos. Sci.*, **64**, 2401–2421.

Rotunno, R. and J. B. Klemp, 1982: The influence of the shear-induced pressure gradient on thunderstorm motion. *Mon. Wea. Rev.*, **110**, 136–151.

Rotunno, R., J. B. Klemp, and M. L. Weisman, 1988: A theory for strong, long-lived squall lines. *J. Atmos. Sci.*, **45**, 463–485.

Schlesinger, R. E., 1973: A numerical model of deep moist convection: Part I. comparative experiments for variable ambient moisture and wind shear. *J. Atmos. Sci.*, **30**, 835–856.

Sherwood, J., 1995: The papal front part 1: A forecaster's perspective. *Wea.*, **50**, 98–106.

University of Wyoming, 2013: Wyoming weather web - atmospheric soundings. http://weather.uwyo.edu/upperair/sounding.html.

Volkert, H., S. P. Ballard, and M. G. Hutchinson, 1995: The papal front part 2: Seen through numerical weather prediction models. *Wea.*, **50**, 134–142.

Volkert, H. and R. Steinacker, 1995: The papal front part 3: Findings from research-type analyses. *Wea.*, **50**, 142–150.

Weisman, M. L. and J. B. Klemp, 1982: The dependence of numerically simulated convective storms on vertical wind shear and buoyancy. *Mon. Wea. Rev.*, **110**, 504–520.

Weisman, M. L. and J. B. Klemp, 1984: The structure and classification of numerically simulated convective stormsin directionally varying wind shears. *Mon. Wea. Rev.*, **112**, 2479–2498.

Wilhelmson, R., 1974: The life cycle of a thunderstorm in three dimensions. *J. Atmos. Sci.*, **31**, 1629–1651.

ZAMG, 2007: ZAMG - monatsrückblick. http://www.zamg.ac.at/cms/de/klima/klima-aktuell/monatsrueckblick/unwetterbericht?monat=08&jahr=2007.

List of Figures

Acknowledgments

I would like to thank my supervisor Univ.-Prof. Dr. Vanda Grubišić for letting me chose a fascinating topic, for her continuous feedback and for the guidance during the whole work. And I am especially grateful for the opportunity to join her research group on mountain meteorology at the University of Vienna. Special thanks goes to Dott. Dott. ric. Stefano Serafin for his help with running the weather model, solving problems with LaTeX and lots of corrections and suggestions.
I would also like to thank Univ.-Prof. Dr. Petra Seibert for her advice and for making it possible to obtain satellite images of the storm system. And of course I thank my colleages from the TM-research group Daniel Leukauf, Johannes Sachsperger, Brigitta Goger, Karin Gruber and Dipl.-Ing. Lukas Strauss for their help and suggestions. I thank Markus Kraft and the Austro Control for providing radar imagery, and also Thomas Schreiner and the European Severe Storms Laboratory for providing severe weather reports for the event. Thanks to the Zentralanstalt für Meteorologie und Geodynamik for providing the station data to verify the simulations.
Thank you to my Parents for supporting me with all my decisions, financing a large part of my time at the university and always encouraging me when I needed it.
Finally, I want to thank the most important person in my life, my girlfriend Karin, for supporting and encouraging me through all this time!

Abstract

The interaction of convective storms with complex terrain is studied through a case study of a convective event, which occurred on 2 August 2007. The goal is to identify the ways in which valleys and mountains influence the development of a convective system. The system of August 2007 moved along the Alpine main ridge for over eight hours, passing over several mountains of over 3000 m in height, which makes it an ideal candidate for this type of research.

The Weather Research and Forecasting Model (WRF) version 3.3 is used to simulate the convective system which ocurred on 2 August 2007. The model is initialized with reanalysis data from the European Center for Medium Range Weather Forecasting. The simulation output is verified by using station data and radar imagery. Distribution of potential temperature and moisture in the valleys and over mountains along the storm track are analyzed to investigate the intensity variations of the supercell's updraft over time. In addition to the real case simulation, two sensitvity tests are conducted, which reduce the topography in two steps. In one simulation the Alps are replaced by a single smooth ridge and in the other simulation the Alps are removed and replaced by a flat plateau with an altitude of 400 m above sea level.

The real case simulation repdroduces a convective system which develops very similar to the observed one. The storm intensity variations agree well with the altitude variations of the underlying terrain and also with the availability of convective available potential energy. Thermal circulation within the convective boundary layer concentrates moisture over convergence zones along ridges and steep slopes, increasing moisture over the whole depth of the planetary boundary layer. This process increases the amount of latent heat in convergence zones. Potential temperature and moisture within and over valleys are not higher than over the surrounding mountains. In fact, the opposite is found, as thermal circulation moves warm air out of the valley. The simulation with smoothed underlying terrain produces a supercell, which exists for only 90 minutes and is not part of a squall line. The sensitivity test without the Alps develops an almost straight cold front with a squall line ahead of the surface cold front and no supercellular development.

The Alps as a whole influenced the wind fields such that wind shear was favourable for supercells. Boundary layer processes are very important for the variations of storm intensity, because the small scale features influenced the storm by supporting a thermal valley circulation which redistributed moisture in the convective boundary layer.

Zusammenfassung

Im Zuge dieser Arbeit wird die Wechselwirkung von Gewittersystemen mit komplexer Topographie untersucht. Zu diesem Zweck wird ein Gewitterereignis, welches am 2. August 2007 auftrat, untersucht. Das Gewittersystem zog von der Ostschweiz über mehr als acht Stunden entlang des Alpenhauptkammes. Es bewegte sich dabei entlang der breiten Längstäler nördlich des Alpenhauptkammes Inntal, Salzachtal und Ennstal und überquerte mehrere Gebirge mit Höhen von bis zu 3000 m mit ca. 14 m s^{-1}.
Das Weather Research and Forecasting (WRF) Modell Version 3.3 wurde verwendet, um das am 2. August aufgetretene Gewittersystem zu simulieren. Die Simulation zeigt die Entwicklung einer Gewitterlinie mit einer Superzelle am Südende und Multizellen am Nordende. Als Grund für die Auslösung des simulierten Gewitters wurde das Zusammenwirken von orographisch induzierter Konvergenz über den Lechtaler Alpen und dem Durchgang einer Konvergenzliene, welche das Resultat nächtlicher Gewitteraktivität und deren Kaltluftseen war. Die Modelldaten werden mit Stationsdaten des TAWES-Messnetzes der Zentralanstalt für Meteorologie und Geodynamik und Raderbildern der Austro Control verglichen.
Die Simulation zeigt, dass Intensitätsschwankungen des Aufwinds eng mit der Geländehöhe unter dem Gewitter zusammenhängen. Die Talwindzirkulation konzentriert die Feuchte in der Grenzschicht in Konvergenzzonen über hohen Bergen oder entlang steiler Hänge. Die potenzielle Temperature und die Feuchte in den Tälern sind nicht höher, als über den Bergen in deren Umgebung. Es ist sogar das Gegenteil zu beobachten, da die Talwindzirkulation warme Luft aus den Tälern bewegt.
Zwei weitere Simulationen wurden durchgeführt, um den Einfluss der Alpen zu ergründen. In einem ersten Schritt wird die Feinstruktur entfernt und die Alpen zu einem einzigen glatten Gebirgszug reduziert. Die Simulation über diesem Gelände produziert eine Superzelle, welche jedoch lediglich 90 Minuten existiert und nicht Teil eines größeren zusammenhängenden Systems ist. Eine weitere Simulation, bei der die Alpen durch ein flaches Plateau auf 400 Metern Seehöhe ersetzt werden, produziert keine Superzelle. Das Ergebnis ist eine Linie aus Gewitterzellen, welche der Kaltfront vorausgeht. Dies zeigt, dass die Alpen als ganzes die Windverhältnisse derart beeinflusst haben, dass Superzellenentwicklung möglich wurde, während die feinere Struktur die Auslösung unterstützt und die Entwicklung beeinflusst haben.

Appendix A

List of Symbols

α	Specific Volume [m^3 kg^{-1}]
b	Buoyancy [kg m s^{-2}]
C	Threshold for Terrain Stretching [m]
c_p	Heat Capacity for Constant Pressure [J kg^{-1} K^{-1}]
e	Partial Pressure of Water Vapor
e_s	Saturation Partial Pressure of Water Vapor
E_{kin}	Kinetic Energy [J kg^{-1}]
f_1	Stretching Function
f_2	Weighting Function
g	Gravitational Acceleration [m s^{-1}]
G	Maximum Height of Stretched Terrain [m]
Γ	Vertical Temperature Lapse Rate
Γ_d	Vertical Dry Adiabatic Lapse Rate
Γ_s	Vertical Pseudoadiabatic Lapse Rate
h	Terrain Height [m]
h_f	Flattened Terrain Height [m]
h_s	Stretched Terrain Height [m]
H	Maximum Height of Terrain [m]
L_c	Latent Heat of Condensation [J kg^{-1}]
M_d	Molar Mass of Dry Air
M_w	Molar Mass of Water
p	Pressure [hPa]
p_s	Surface Pressure [hPa]
q	Specific Humidity [g kg^{-1}]
q_s	Saturation Specific Humidity [g kg^{-1}]
q_v	Water Vapor Mixing Ratio [g kg^{-1}]
R	Specific Gas Constant [J kg^{-1} K^{-1}]
ρ	Density [kg m^{-3}]
ρ_d	Density of Dry Air [kg m^{-3}]
ρ_v	Density of Water Vapor [kg m^{-3}]
RH	Relative Humidity [%]

T	Temperature [K] or [°C]
T_d	Dewpoint [K] or [°C]
θ	Potential Temperature [K]
θ_e	Equivalent Potential Temperature [K]
θ_e^*	Saturation Equivalent Potential Temperature [K]
w	Vertical Velocity [m s^{-1}]

List of Acronyms

ASL	Above Sea Level
AGL	Above Ground Level
CAPE	Convective Available Potential Energy
CIN	Convective Inhibition
ECMWF	European Centre for Medium-Range Weather Forecasts
FFD	Front Flank Downdraft
LMS	Left Moving Storm
RFD	Rear Flank Downdraft
RMS	Right Moving Storm
TAWES	Teilautomatisches-Wetter-Erfassungs-System
ZAMG	Zentralanstalt für Meteorologie und Geodynamik

Appendix B

Conversions and Corrections for Easier Comparability

The TAWES stations used by the ZAMG report relative humidity RH or dewpoint T_d - sometimes even both or none at all - while the model output data contains the specific humidity q_v which is the mass of water vapor per kg of moist air. In order to compare moisture from measurements and model output, the model output will be converted into RH and T_d. To calculate the saturated water vapor pressure for a given temperature T, the approximation of Murray (1967)

$$e_s = 6.1078e^{\frac{17.2693882(T-273.16)}{T-35.86}} \tag{1}$$

will be used. The formula is a good choice since it is a reasonable approximation with the error being less than two percent within the temperature range observed in the case study. It can also be tramsformed relatively easy to obtain T_d for a given saturation water vapor pressure e.

$$T_d = \frac{17.2693882 \cdot 273.16 - 35.86 \ln\left(\frac{e_s}{6.1078}\right)}{17.2693882 - \ln\left(\frac{e_s}{6.1078}\right)} \tag{2}$$

From the water vapor mixing ratio q_v we can obtain the partial pressure of water vapor e by using

$$q_v = \frac{\rho_v}{\rho} = \frac{\rho_v}{\rho_d + \rho_v} \tag{3}$$

along with the ideal gas law $p\alpha = RT$ and $R_s = \frac{R_m}{M_s}$ where R_s is the specific gas constant, R_m is the universal or molar gas constant and M_s is the molar mass, we obtain

$$q_v = \frac{M_w e}{M_d(p-e) + M_w e} = \frac{\frac{M_w}{M_d} e}{p - \left(1 - \frac{M_w}{M_d}\right) e}, \tag{4}$$

where $M_d \approx 28.964$ g mol^{-1} (American Meteorological Society, 2012) is the molar mass of dry air in the standard atmosphere and $M_w \approx 18.016$ g mol^{-1} (Holton, 2004, p. 491) is the molar mass of water. Since e/p is usually $\mathcal{O}(10^{-2})$, this leads to the simple approximation

$$q_v = \frac{0.622e}{p - 0.378e} \approx 0.622\frac{e}{p} \Leftrightarrow e \approx \frac{q_v p}{0.622}. \tag{5}$$

Thus, T_d and RH can be calculated from the model variables p and q_v. Any values for T_d and RH from the model output given below are calculated using the above approximations.

The surface pressure was corrected by adding a constant Δp which was obtained from the altitude difference between the real station and the closest grid point in the model data. The expected Δp is calculated using the international standard atmosphere for which $p(h)$ is given by

$$p(h) = 1013.25 \cdot \left(1 - \frac{0.0065 \cdot h}{288.15}\right)^{5.255} \text{hPa}, \tag{6}$$

where h is the height ASL and $\Delta p = p(h_{real}) - p(h_{model})$ is added to the model's pressure. This method is by no means accurate but it helps to reduce the gap between the model and real pressure time series. It reduces the gap to an order of magnitude which is similar to that of the variations over time, improving their visibility.

Appendix C - Map

Map of Relevant Geographic References

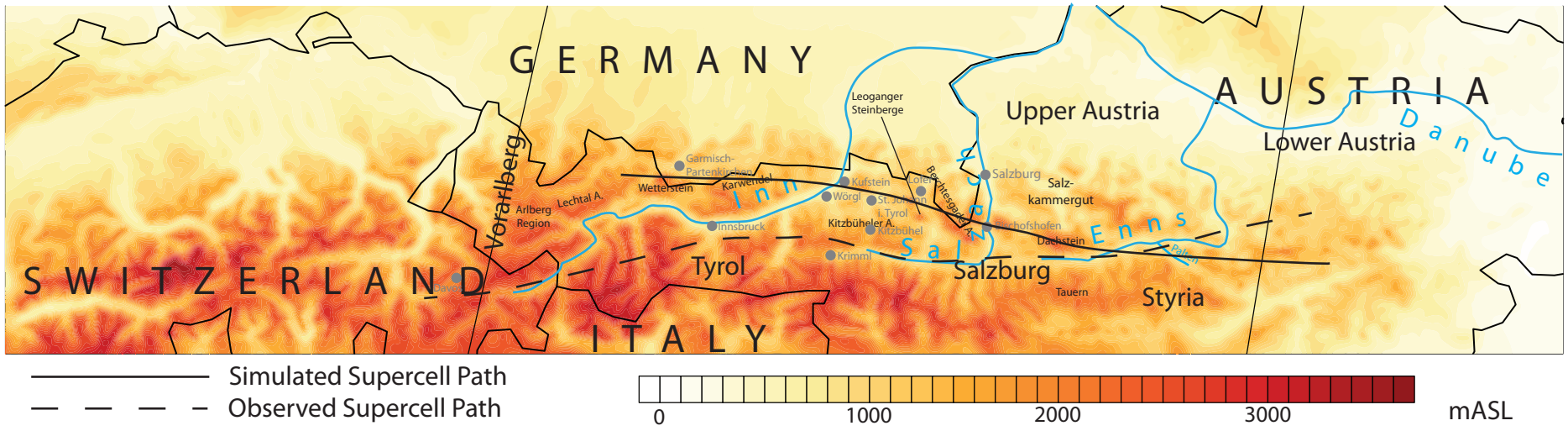

Figure 1: Map of relevant geographical references with simulated and observed supercell storm tracks overlaid.

Phillip Scheffknecht

Bildungsweg

2012	Besuch der 4th ISAC Summer School on Severe Convective Weather
2010	Segelflugmeteorologische Exkursion in Lanzen/Thurnau
Seit 2006	Studium Meteorologie an der Universität Wien

Bisherige Tätigkeiten

Seit 2012	Mitglied der Forschungsgruppe für Theoretische Meteorologie am Institut für Meteorologie der Universität Wien

Wissenschaftlicher Werdegang

2012	Poster *The Simulation of Convective Storms over Idealized Terrain* – 4th ISAC Summer School in Castro Marina, Italien